Institutionen för systemteknik
Department of Electrical Engineering

Examensarbete

UKF and EKF with time dependent measurement and model uncertainties for state estimation in heavy duty diesel engines

Examensarbete utfört i Fordonssystem
vid Tekniska högskolan vid Linköpings universitet
av

Henrik Berggren & Martin Melin

Linköpings universitet
TEKNISKA HÖGSKOLAN

Department of Electrical Engineering	Linköpings tekniska högskola
Linköpings universitet	Linköpings universitet
SE-581 83 Linköping, Sweden	581 83 Linköping

UKF and EKF with time dependent measurement and model uncertainties for state estimation in heavy duty diesel engines

Henrik Berggren & Martin Melin

	Avdelning, Institution Division, Department Division of Vehicular Systems Department of Electrical Engineering Linköpings universitet SE-581 83 Linköping, Sweden	**Datum** Date 2011-06-14

Titel Title	UKF och EKF med tidsberoende mät- och modellosäkerheter för tillståndsskattningar i tunga dieselmotorer UKF and EKF with time dependent measurement and model uncertainties for state estimation in heavy duty diesel engines

Författare Author	Henrik Berggren & Martin Melin

Sammanfattning
Abstract

The continuous challenge to decrease emissions, sensor costs and fuel consumption in diesel engines is battled in this thesis. To reach higher goals in engine efficiency and environmental sustainability the prediction of engine states is essential due to their importance in engine control and diagnosis. Model output will be improved with help from sensors, advanced mathematics and non linear Kalman filtering. The task consist of constructing non linear Kalman Filters and to adaptively weight measurements against model output to increase estimation accuracy. This thesis shows an approach of how to improve estimates by nonlinear Kalman filtering and how to achieve additional information that can be used to acquire better accuracy when a sensor fails or to replace existing sensors. The best performing Kalman filter shows a decrease of the Root Mean Square Error of 75% in comparison to model output.

Abstract

The continuous challenge to decrease emissions, sensor costs and fuel consumption in diesel engines is battled in this thesis. To reach higher goals in engine efficiency and environmental sustainability the prediction of engine states is essential due to their importance in engine control and diagnosis. Model output will be improved with help from sensors, advanced mathematics and non linear Kalman filtering. The task consist of constructing non linear Kalman Filters and to adaptively weight measurements against model output to increase estimation accuracy. This thesis shows an approach of how to improve estimates by nonlinear Kalman filtering and how to achieve additional information that can be used to acquire better accuracy when a sensor fails or to replace existing sensors. The best performing Kalman filter shows a decrease of the Root Mean Square Error of 75% in comparison to model output.

Sammanfattning

Minskning av utsläpp och sensorkostnader samt låg bränsleförbrukning i tunga dieselmotorer behandlas i denna avhandling. För att nå högre mål i motoreffektivitet och hållbar utveckling är estimering av motorns tillstånd avgörande då det spelar en väsentlig roll vid motorstyrning och diagnos. En modells utsignaler kommer att förbättras med hjälp av sensorer, avancerad matematik och Kalmanfiltrering. Uppgiften består av att konstruera ickelinjära Kalmanfilter och adaptivt vikta mätningar mot modellens utsignaler för att öka estimeringsnoggrannheten. Denna avhandling visar på hur man kan förbättra modellbaserade estimeringar med hjälp av Kalmanfiltrering och hur man kan erhålla ytterliggare information för att öka precisionen då en sensor går sönder eller ersätta existerande sensorer. Det bäst presterande filtret ger en minskning av kvadratroten ur medelkvadratavvikelsen (RMSE) på 75 % i jämförelse med modellens utsignaler.

Acknowledgments

This thesis is the result of 20 weeks of research, discussions, and hard work at Scania CV AB in Södertälje. We have enjoyed the working environment with encouraging and friendly colleagues and interesting discussions during the "fika"-breaks in building 107. Our supervisor Erik Höckerdal and examiner Assoc. Prof. Erik Frisk have been of great assistance providing ideas, inspiration and guidance, for which we are truly grateful. We would like to mention our fellow thesis colleagues at NESE who made every day at Scania a bit more enjoyable. We also want to declare our appreciation to Scania for giving us insight to a large organisation, the opportunity to observe daily working methods and conditions in "the real world" and the enormous amount of provided non work related activities, such as tennis, floorball, petanque etc.

We would also like to express our mixed emotions about restaurant "270" which we have visited almost every Thursday during this semester. Thanks for the delicious pancakes and dishes, which unfortunately often resulted in unproductive Thursday afternoons.

Finally we would like to thank our friends and families for all their love and support.

Contents

Chapter 1

Introduction

The development in the heavy truck industry is driven by emission legislators and the customer's demand on low fuel consumption. The control and diagnostic systems are fundamental in reducing emissions and constructing efficient engines. In order to successfully control engines and to maintain reliable diagnosis systems, accurate information of the engine states is essential. To reach the emission limits with low fuel consumption, concepts like Exhaust Gas Recirculation (EGR) and Variable Geometry Turbines (VGT) are introduced, [15]. By increasing the intake manifold EGR fraction X_{egr}, NO_x emissions are reduced and by maintaining a high enough oxygen/fuel ratio λ, smoke generation is avoided. X_{egr} and λ are thus often used as performance variables when minimizing engine emissions. Estimates can be obtained using sensors inside the engine that measure the engine states, or from engine models. The sensor costs for purchase, installation and repair become important as the quantity of sold engines increase. With model based estimates, sensors can be replaced or their accuracy increased through the given additional information. Therefore the attention on model based estimation increase.

1.1   Purpose and Goal

To construct a general engine model that fulfils the need of rigorous state estimations, is difficult if not even unattainable. The purpose of this work is to investigate to what extent, the model based estimates in an engine, can be improved with help from sensors, advanced mathematics, regular non-linear Kalman filtering and adaptive non-linear Kalman filtering. The goal is to obtain accurate estimates of λ and X_{egr}. A DAE based Extended Kalman Filter (EKF) will be compared to an ODE based Unscented Kalman Filter (UKF). An adaptation of the best performing filter will be made in an attempt to further improve the estimates. The adaptation will be made with help from information of the model and measurement accuracy during different control signal intervals. This information is used while adapting the covariance matrices of model and measurement noise. The possibility of replacing sensors with the estimates from the Kalman filtered estimates will also be investigated.

1.2   Problem Statement

To improve model based estimates, different problems must be dealt with. To improve the estimation accuracy, Kalman filtering is used. This leads to the problem of how to implement and tune the filters. The filters are tuned by weighting measurements against model based estimates, this is done by assigning the measurement noise and state prediction noise certain covariances, R and Q. It must be investigated in which operating points the model gives inaccurate state estimates. How the R and Q should be adapted for these operating points to further improve the estimates is the next problem. The number of operating points is large so they need to be divided into appropriate subsets of operating points. One subset is supposed to correspond to one covariance setting, which is the topic of Chapter 7. The Problem statement can be clarified in the following sub problems:

1. How should the filters be implemented?

2. What weighting should be chosen for the Kalman filters? i.e. ordinary Kalman tuning without any kind of adaptation (choose R and Q matrices).

3. What subsets of operating points should be chosen? i.e. what operating points show similar behaviour for the estimates and can therefore be grouped in the same subset.

4. What should the adaptive weighting ($R(t)$ and $Q(t)$) be for the different subsets?

5. The implementation of the UKF and EKF should be robust, what can be made to increase the stability of the systems?

Chapter 2

Earlier Work

A brief description of earlier work will be presented in this Chapter, such as the engine model and efforts to improve it.

2.1 Model of Diesel Engine

The studied model is a six cylinder diesel engine model with intake throttle, VGT and EGR, made by Johan Wahlström and presented in [18].

2.1.1 Short description:

The engine model is a mean value model, from actuator input to system output, with the objective to describe the dynamics of the intercooler pressure, manifold pressures, turbocharger and EGR. An illustration of the model can be viewed in Figure 2.1.
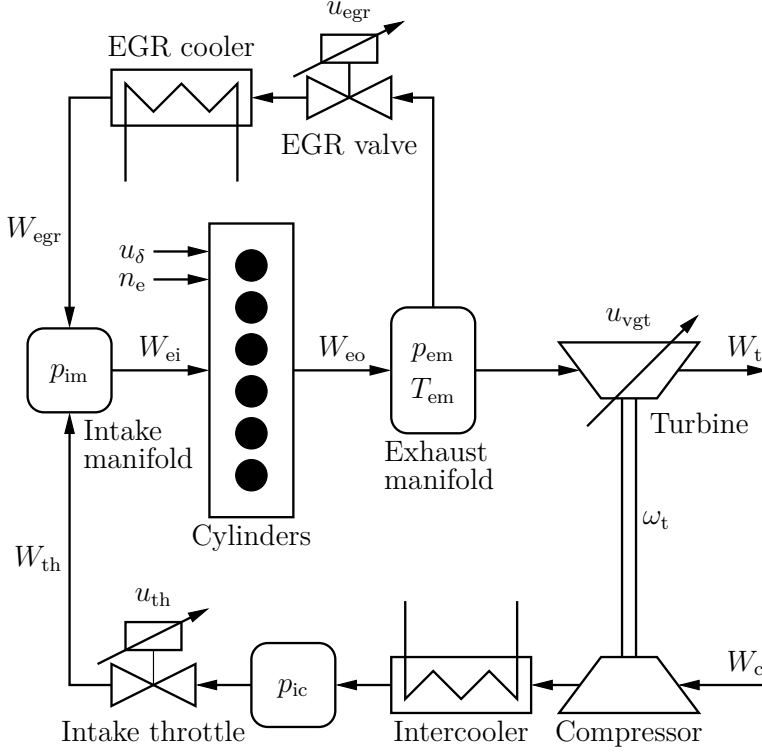
Figure 2.1. Schematic of the diesel engine model [18] with intake manifold throttle, EGR, and VGT, showing model states (p_{im}, p_{em}, p_{ic}, ω_t, and T_{em}), control inputs (u_{egr}, u_{vgt}, u_δ, and u_{th}), parametrization input (n_e), and flows between the different components (W_c, W_{th}, W_{egr}, W_{ei}, W_{eo}, and W_t). Rectangles with rounded corners represent control volumes.

2.1.2 The model in state space form:

The model has the following states: intercooler, intake manifold and exhaust manifold pressures (p_{ic}, p_{im}, p_{em}), oxygen mass fraction in the intake and exhaust manifold (X_{Oim}, X_{Oem}), exhaust manifold temperature (T_{em}) and turbocharger speed (ω_t). That is,

$$x = (p_{ic}, p_{im}, p_{em}, T_{em}, X_{Oim}, X_{Oem}, \omega_t)^T, \tag{2.1}$$
$$\dot{x} = f(x, u, n_e), \tag{2.2}$$

where n_e is a parametrization input and u is the actuator position vector. In Equation 2.3 $\dot{x}$ is presented followed by a measurement presentation in 2.4.

$$
\begin{aligned}
\dot{p}_{\mathrm{im}} &= f_{p_{\mathrm{im}}} && (p_{\mathrm{im}}, && p_{\mathrm{em}}, && p_{\mathrm{ic}}, && && T_{\mathrm{em}}, && u_\delta, && u_{\mathrm{egr}}, && && u_{\mathrm{th}}, && n_{\mathrm{e}}) \\
\dot{p}_{\mathrm{em}} &= f_{p_{\mathrm{em}}} && (p_{\mathrm{im}}, && p_{\mathrm{em}}, && && \omega_{\mathrm{t}}, && T_{\mathrm{em}}, && u_\delta, && u_{\mathrm{egr}}, && u_{\mathrm{vgt}}, && && n_{\mathrm{e}}) \\
\dot{p}_{\mathrm{ic}} &= f_{p_{\mathrm{ic}}} && (p_{\mathrm{im}}, && && p_{\mathrm{ic}}, && \omega_{\mathrm{t}}, && && && && && u_{\mathrm{th}} &&) \\
\dot{\omega}_{\mathrm{t}} &= f_{\omega_{\mathrm{t}}} && (&& p_{\mathrm{em}}, && p_{\mathrm{ic}}, && \omega_{\mathrm{t}}, && T_{\mathrm{em}}, && && && u_{\mathrm{vgt}} && &&) \\
\dot{T}_{\mathrm{em}} &= f_{T_{\mathrm{em}}} && (p_{\mathrm{im}}, && p_{\mathrm{em}}, && && \omega_{\mathrm{t}}, && T_{\mathrm{em}}, && u_\delta, && u_{\mathrm{egr}}, && u_{\mathrm{vgt}}, && && n_{\mathrm{e}}) \\
\dot{X}_{O_{em}} &= f_{X_{O_{em}}} && (&& p_{\mathrm{em}}, && && \omega_{\mathrm{t}}, && T_{\mathrm{em}}, && && u_{\mathrm{egr}}, && u_{\mathrm{vgt}}, && &&) \\
\dot{X}_{O_{im}} &= f_{X_{O_{em}}} && (p_{\mathrm{im}}, && && && \omega_{\mathrm{t}}, && T_{\mathrm{em}}, && && u_{\mathrm{egr}}, && u_{\mathrm{vgt}}, && &&)
\end{aligned} \tag{2.3}
$$

$$
\begin{aligned}
y_1 &= p_{\mathrm{im}} && \text{(2.4a)} \\
y_2 &= p_{\mathrm{em}} && \text{(2.4b)} \\
y_3 &= p_{\mathrm{ic}} && \text{(2.4c)} \\
y_4 &= \omega_{\mathrm{t}} && \text{(2.4d)} \\
y_5 &= W_{\mathrm{c}} \left(p_{\mathrm{ic}}, \quad \omega_{\mathrm{t}} \right) && \text{(2.4e)}
\end{aligned}
$$

Appendix B contains a summary of the model equations while a complete description is found in [18].

2.1.3 Model Evaluation:

The model has been validated against measurements from the World Harmonized Transient Cycle (WHTC), [14]. During the engine simulation of the WHTC, *EGR* is not active. In Figure 2.2, one can observe a simulation based on data with active *EGR* and the result differ from the measurements. Opened *VGT*, fast changes in throttle position and high amount of injected fuel affect the predictions negative. This indicates that the model predicts the states poorly during these circumstances. The weaknesses of the model will be explained more thorough in Chapter 5.
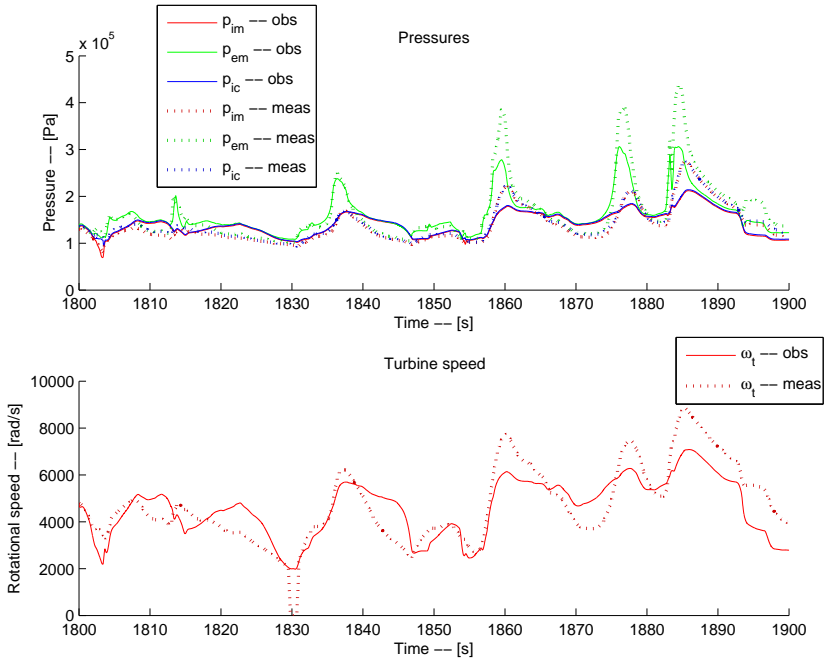
Figure 2.2. Plots of the model based estimates of pressures and turbine speed.

2.2 EKF of ODE and DAE models

Efforts have been made to improve the model based estimates and to decrease the computational complexity of the EKF. In Höckerdal et al. [8], the Ordinary Differential Equation (ODE) of the model is compared to the ODE transformed into a Differential Algebraic Equation (DAE). Both model outputs are filtered with the Extended Kalman Filter (EKF) and the DAE model is shown to give better estimation performance with less computational effort. The DAE model is also shown to be more robust than the ODE model, hence the DAE model is used in this thesis.

Chapter 3

Methods and stability: EKF vs UKF

In this chapter the theory behind efforts to improve the model based estimates is explained. The implementations of the EKF and UKF are presented as well as different discretisation methods used in the implementations.

3.1 EKF

The Kalman Filter was first presented by Rudolf E. Kalman in 1960 [11]. The purpose of the Kalman Filter is to minimize the covariance of the estimation error. The Kalman Filter was originally developed for linear models, but later developed to also be suitable for non linear models. The Extended Kalman Filter (EKF) is the most used filter for non linear models and is used in various fields, e.g. for chemical engineering processes, see [12]. A thorough presentation of the Kalman Filter and nonlinear extensions can be found in [16]. An overview of the EKF is shown in Figure 3.1.

3.1.1 EKF Theory

In the Extended Kalman Filter a linearisation of the non-linear model is made around the best state estimate available, i.e. the latest estimate, the Kalman equations are then applied to compute a new estimate. The differential equations are, for this implementation, solved numerically by using the Classical Runge Kutta, Backward Euler or Forward Euler method. The EKF use noise covariance matrices R and Q as a priority between trusting the model and the measurements. The EKF is presented more detailed in [6, 16].

EKF of DAE

In Höckerdal et al. [8] the ODE engine model is transformed into a DAE model. This is done by approximating the pressure change over the intercooler as constant.
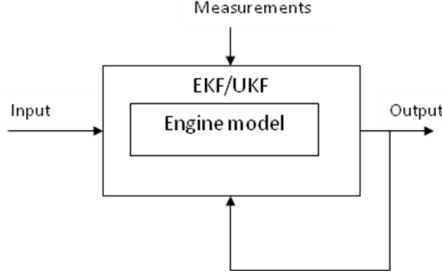
Figure 3.1. EKF overview.

This results in a DAE model where the pressure in the intercooler p_{ic} is an algebraic variable. The DAE is solved according to the description in Becerra et al. [17], which is similar to an EKF algorithm of an ODE with an additional update for the intercooler pressure p_{ic}. Due to the computational and stability benefits shown in höckerdal et al. [8] the DAE model is used in this thesis. The DAE model is described in the following way,

$$
\begin{aligned}
\dot{x} &= f(x, z, u, n_e), \\
0 &= g(x, z, u, n_e), \\
y &= h(x, z, u),
\end{aligned}
$$

where x and z are the differential and algebraic variables. Since only the dynamic states are included in the EKF calculations the estimation quality of the algebraic states is not used while calculating the Kalman gain. This is solved by differentiating the linearized algebraic subsystem and including them in the EKF algorithm, see [12] and Equations 3.1 and 3.2.

$$
\begin{aligned}
\dot{x} &= A_t x + B_t z \\
0 &= C_t x + D_t z
\end{aligned}
\quad \Rightarrow \quad
\begin{aligned}
\dot{x} &= A_t x + B_t z, \\
\dot{z} &= -D_t^{-1} C_t \dot{x},
\end{aligned}
\tag{3.1}
$$

where

$$
\begin{pmatrix} A_t & B_t \\ C_t & D_t \end{pmatrix} = \begin{pmatrix} \frac{\delta f}{\delta x} & \frac{\delta f}{\delta z} \\ \frac{\delta g}{\delta x} & \frac{\delta g}{\delta z} \end{pmatrix}.
\tag{3.2}
$$

The algorithm for EKF based on DAE is shown in Algorithm 1 and in [8]. It uses the Forward Euler method to discretize the model, see Equation 3.3. The method is explained in Section 3.3.1.

Algorithm 1: EKF Algorithm of DAE

---

1. Initiate the filter by approximating the following:

$$\hat{x}_{0|-1} = x_0 \text{ and } P_{0|-1} = P_0,$$

where x_0 is the initial state estimate and P_0 the covariance matrix of x_0. Let $t = 0$.

2. Measurement Update:

$$
\begin{aligned}
\hat{x}_{t|t} &= \hat{x}_{t|t-1} + \bar{K}_t(y_t - h(\hat{x}_{t|t-1})), \\
0 &= g(\hat{x}_{t|t}, \hat{z}_{t|t}, u_{t|t}, n_e) \Rightarrow \hat{z}_{t|t}, \\
P_{t|t} &= (I - K_t H_t)P_{t|t-1}, \\
K_t &= P_{t|t-1}H_t^T(H_t P_{t|t-1}H_t^T + R_t)^{-1},
\end{aligned}
$$

where the implication arrow indicates that $\hat{z}_{t|t}$ has been obtained by solving the equation $g = 0$ and H is the gradient $h_x(\hat{x}_{t|t-1})$ (numerically computed).

3. Time Update:

$$
\begin{aligned}
\hat{x}_{t+1|t} &= \hat{x}_{t|t} + T_s f(\hat{x}_{t|t}, \hat{z}_{t|t}, u_{t|t}) \\
0 &= g(\hat{x}_{t|t}, \hat{z}_{t|t}, u_{t|t}, n_e) \Rightarrow \hat{z}_{t+1|t} \\
\bar{P}_{t+1|t} &= \bar{A}_{t|t} P_{t|t} \bar{A}_{t|t}^T + \bar{G}_{t|t} \bar{Q}_t \bar{G}_{t|t}^T,
\end{aligned}
\tag{3.3}
$$

where

$$\bar{A}_{t|t} = I + T_s \begin{pmatrix} A_{t|t} & B_{t|t} \\ D_{t|t}^{-1}C_{t|t}A_{t|t} & D_{t|t}^{-1}C_{t|t}B_{t|t} \end{pmatrix},$$

T_s denotes the discretization step length, and

$$\bar{G}_{t|t} = \begin{pmatrix} I \\ -D_{t|t}^{-1}C_{t|t} \end{pmatrix}$$

4. Let $t := t + 1$ and repeat from 2.

3.2   Unscented Kalman Filter

The UKF was introduced by Julier et al. in [9] year 1995 in an attempt to improve Kalman filtering for non linear models. Several papers have presented results where UKF outperforms EKF e.g [3] and [2].

3.2.1   Differences between UKF and EKF

The EKF is based on linearisation of nonlinear systems and might perform poorly for highly nonlinear systems. The EKF also has to compute Gradients (Jacobian matrices), that may lead to heavy computations and numerical inaccuracy. In the UKF no gradients are required and therefore some of the EKF's disadvantages are avoided. The UKF propagate the noise through the actual nonlinear functions (see Unscented Transform in Section 3.2.2) and avoids the flaws of linear approximation. These benefits of the UKF encouraged an investigation of the UKF's ability to improve the state estimates compared to the EKF.

3.2.2   Unscented Transform

The fundamental idea of the UKF is to use a set of carefully chosen points (sigma points) to describe the estimation error statistics and propagate them through the nonlinear functions. This is done to capture the effect of model nonlinearities on the estimation error statistics during estimation. This transform of the distribution is called the Unscented Transform. A description of the selection of sigma points and the unscented transform of a distribution x follows, see Equations 3.4 to 3.9.

$$\textbf{Distribution of x:} \quad x^{(i)} \sim N(\mu_x, P), \quad i = 1, ..., N. \tag{3.4}$$

$$\textbf{Select sigma points:} \quad x^{(0)} = \mu_x, \qquad x^{(\pm i)} = \mu_x \pm \sqrt{n_x + \lambda^{ukf}} \sigma_i u_i. \tag{3.5}$$

Singular Value Decomposition (SVD) of the covariance matrix P, see [7], is used to calculate u_i and σ_i.

$$P = U\Sigma U^T = \sum_{i=1}^{n_x} \sigma_i^2 u_i u_i^T. \tag{3.6}$$

The sigma points are mapped through the non-linear system $y^i = g(x^i)$ and the resulting mean and covariance can be calculated with:

$$\hat{y} = \sum_{i=-n_x}^{n_x} \omega^{(i)} y^{(i)}, \tag{3.7}$$

$$P_y = \sum_{i=-n_x}^{n_x} \omega^{(i)} (y^{(i)} - \hat{y})(y^{(i)} - \hat{y})^T$$
$$+ (1 - \alpha^2 + \beta)(y^{(0)} - \hat{y})(y^{(0)} - \hat{y})^T, \tag{3.8}$$

where $\omega^{(i)}$ are weights and can be chosen in various ways, for instance:

$$\omega^{(0)} = \frac{\lambda^{ukf}}{n_x + \lambda^{ukf}}, \quad \omega(\pm i) = \frac{1}{2(n_x + \lambda_{ukf})}. \tag{3.9}$$
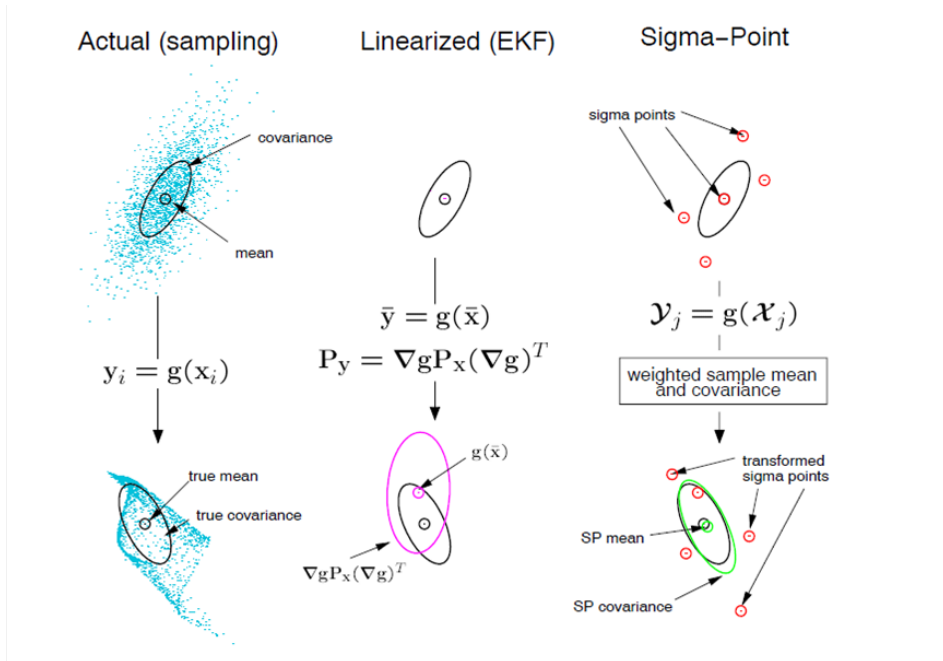
Figure 3.2. Mean and Covariance estimation for EKF (linearisation) and UKF (Unscented Transform), picture is from [13]

Figure 3.2 show how the sigma points are mapped through the non-linear system $g(x)$ and comparing its estimation of state statistics with a linearised estimation of state statistics and with the actual state statistics. The parameters in Table 3.1, first presented by Wan et al. [1], are used in the UKF, where α is the primary scaling factor for the distance between the sigma points and $x^{(0)}$, and β a distribution compensation taking care of higher order statistic effects. Other choices of parameters are presented in [10].

Table 3.1. UKF Parameters

Parameter	value
α	10^{-3}
β	2
λ_{ukf}	$\alpha^2 n_x - n_x$
$\sqrt{n_x + \lambda_{ukf}}$	$10^{-3}\sqrt{n_x}$

Algorithm 2: UKF Algorithm

---

1. Initiate the states and the state covariance with initial condition:

$$\hat{x}_{0|-1} = x_0 \quad \text{and} \quad P_{0|-1} = P_0,$$

where x_0 is the initial state estimate and P_0 the covariance matrix of x_0. Let $t = 0$.

2. Choose N sigma points $(\chi_{e_t}^i)$ for the augmented state vector:

$$\chi_{e_t} = \begin{pmatrix} x_t \\ e_t \end{pmatrix} \sim \mathcal{N} \left(\begin{pmatrix} \hat{x}_{t|t-1} \\ 0 \end{pmatrix}, \begin{pmatrix} P_{t|t-1} & 0 \\ 0 & R_t \end{pmatrix} \right).$$

$N = 2n_{\chi_{e_t}} + 1$, where $n_{\chi_{e_t}}$ is the order of the augmented state vector $\chi_{e_t}^i$ and e_t measurement noise.

3. Measurement update:

$$\begin{aligned}
\hat{x}_{t|t} &= \hat{x}_{t|t-1} + P_{t|t-1}^{xy} P_{t|t-1}^{-yy}(y_t - \hat{y}_t), \\
P_{t|t} &= P_{t|t-1} - P_{t|t-1}^{xy} P_{t|t-1}^{-yy} P_{t|t-1}^{xyT},
\end{aligned}$$

where

$$\begin{aligned}
y_t^{(i)} &= g(x_{t|t-1}^{(i)}, e_t^{(i)}), \\
\hat{y}_t &= \sum_{i=0}^{N} \omega_{m,t}^{(i)} y_t^{(i)}, \\
P_{t|t-1}^{yy} &= \sum_{i=0}^{N} \omega_{c,t}^{(i)} (y_t^{(i)} - \hat{y}_t)(y_t^{(i)} - \hat{y}_t)^T + \\
&\quad + (1 - \alpha^2 + \beta)(y^{(0)} - \hat{y})(y^{(0)} - \hat{y})^T, \\
P_{t|t-1}^{xy} &= \sum_{i=0}^{N} \omega_{c,t}^{(i)} (x_{t|t-1}^{(i)} - \hat{x}_{t|t-1})(y_t^{(i)} - \hat{y}_t)^T.
\end{aligned}$$

4. Choose N sigma points $(\chi_{w_t}^i)$ for the augmented state vector:

$$\chi_{w_t} = \begin{pmatrix} x_t \\ w_t \end{pmatrix} \sim \mathcal{N} \left(\begin{pmatrix} \hat{x}_{t|t} \\ 0 \end{pmatrix}, \begin{pmatrix} P_{t|t} & 0 \\ 0 & Q_t \end{pmatrix} \right).$$

$N = 2n_{\chi_{w_t}} + 1$, where $n_{\chi_{w_t}}$ is the order of the augmented state vector $\chi_{w_t t}^i$ and w_t process noise.

5. Time update:

$$\begin{aligned}
\hat{x}_{t|t-1} &= \sum_{i=0}^{N} \omega_t^{(i)} x_{t|t-1}^{(i)}, \\
P_{t+1|t} &= \sum_{i=0}^{N} \omega_t^{(i)} (x_{t|t-1}^{(i)} - \hat{x}_{t|t-1})(x_{t|t-1}^{(i)} - \hat{x}_{t|t-1})^T,
\end{aligned}$$

where

$$x^{(i)}_{t|t-1} \quad = \quad f(x^{(i)}_{t-1|t-1}, w^{(i)}_t). \tag{3.10}$$

6. Let $t = t + 1$ and repeat from 2.

3.3   Discretistaion Methods

Three different discretisation methods will be evaluated in this thesis. The disctretisation is used when the state $\hat{x}_{t+1|t}$ is predicted, i.e. in Equation 3.3 and 3.10. The Forward Euler (FE) method and Backward Euler (BE) method are treated in Höckerdal et al. [8]. The third alternative investigated is the classical Runge Kutta (RK) method.

3.3.1   Forward Euler

The Forward Euler method is simple, explicit and easy to implement. It uses the current estimate $\hat{x}_{t|t}$, its derivative $f(\hat{x}_{t|t}, u, n_e)$ and the step length $\triangle T$ to predict the next estimate, see Equation 3.11. The stability of the FE method might be lost if the step length is too large.

$$\dot{x} = f(\hat{x}_{t|t}, u, n_e) \approx \frac{\hat{x}_{t+1|t} - \hat{x}_{t|t}}{\triangle T} \Rightarrow \hat{x}_{t+1|t} \approx \hat{x}_{t|t} + \triangle T f(\hat{x}_{t|t}, u, n_e). \tag{3.11}$$

3.3.2   Backward Euler

The Backward Euler method is, unlike the FE method, implicit. It is stable also for larger step lengths but is computationally more demanding since a number of iterations must executed to obtain the solution. An expression of the BE method is shown in Equation 3.12.

$$\dot{x} = f(\hat{x}_{t+1|t}, u, n_e) \approx \frac{\hat{x}_{t+1|t} - \hat{x}_{t|t}}{\triangle T} \Rightarrow \hat{x}_{t+1|t} \approx \hat{x}_{t|t} + \triangle T f(\hat{x}_{t+1|t}, u, n_e). \tag{3.12}$$

3.3.3   classical Runge Kutta

Due to the slow execution of the BE method and less stable FE method, the Runge Kutta (RK) method is investigated. With the RK method, the inverse matrix calculation of the BE method is avoided and the result corresponds to a higher order Taylor expansion than in the FE method. The Runge Kutta method was developed by M.W. Kutta and C.Runge around 1900 and is presented in Algorithm 3.

Algorithm 3: Runge Kutta Algorithm

---

1. Consider the ordinary differential equation f and the initial state x_0:

$$\dot{x} = f(t, x)$$
$$x(0) = x_0,$$

2. Use a weighted average of approximated values of $f(t, x)$ at different times:

$$
\begin{aligned}
t_{n+1} &= t_n + h \\
x_{n+1} &= x_n + (1/6)(k_1 + 2k_2 + 2k_3 + k_4),
\end{aligned}
$$

where,

$$
\begin{aligned}
k_1 &= hf(t_n, x), \\
k_2 &= hf(t_n + h/2, x + k_1/2), \\
k_3 &= hf(t_n + h/2, x + k_2/2), \\
k_4 &= hf(t_n + h, x + k_3).
\end{aligned}
$$

3.4 Model and Filter stability

The EKF and especially the UKF are not very robust in their original implementations. The model suffer from big differences in fast and slow dynamics which can make the system diverge in some operating points. This has been compensated for in the DAE model by approximating the fast dynamics (intercooler pressure) with instantaneous relations [8]. This remodelling has made the model more robust but with the result of less accurate state estimates during changes in the throttle control signal. This is because changes in throttle position will create, for the DAE model, a direct air mass flow change into the intercooler with a subsequent pressure change over the intercooler. The turbine speed sensor can not detect turbine rotational speed under 2094 rad/sec, i.e. the sensor reading is 0 for speeds below 2094 rad/s. This drop can cause the filters to diverge. A way to avoid these divergences is to exclusively trust the model when the turbine rotational speed is below 2094 rad/sec. Finally the covariance matrices should be symmetric but because of numerical inaccuracy some matrix elements can differ a bit which can cause instability. In order to ensure symmetric covariance matrices and make the system more stable non symmetric covariance matrices are eliminated by the operation: $P = \frac{P + P^T}{2}$.

Chapter 4

Validation Methods

The validations of the efforts to improve the model based estimates, is explained in this chapter. Different validation measures and validation quantities will be presented and discussed. The validation data comes from an inline 6 cylinder engine with EGR, VGT and intake throttle. The data is from a drive during the winter tests in Arjeplog 2011. The following control signals: Engine speed, Injected fuel, EGR, Intake Throttle and VGT are used for all validations and are plotted in Figure 4.1.

4.1   Bus validation

The engine model in [18] is adjusted for a diesel engine for trucks. The only vehicle with the right set-up of logged signals (control signals and sensor data) with the right engine that could be found in Scanias data bank, was a bus. The bus engine is the same as the modelled engine but with the difference of a bigger control volume for the intake manifold on the bus. This has been compensated for in the model by increasing V_{im} from 0.0351 m^3 to 0.042 m^3, see Appendix B.

4.2   Validation Measures

Two different validation measures will be used, Root Mean Square Error ($RMSE$) and estimation error histograms, where the latter is used as an estimate of the estimation error statistics.
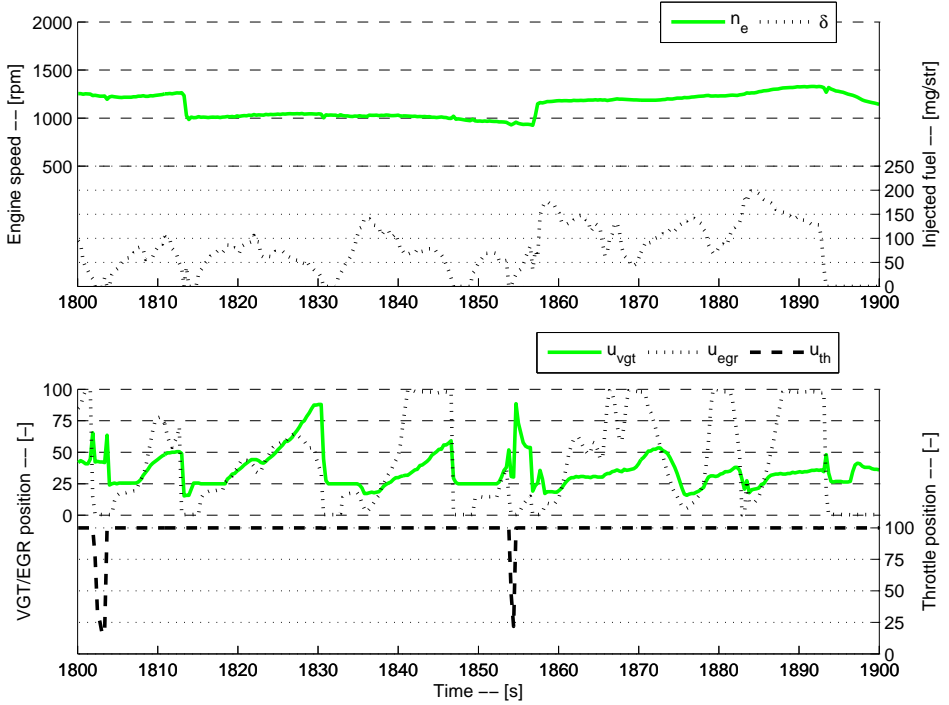
Figure 4.1. Plots of the control signals during the evaluation interval 1800-1900 s.

4.2.1   Root Mean Square Error

The Root Mean Square Error ($RMSE$) is the square root of the variance of the error, see [5]. It indicates how close the estimated values are to the measured values. Since the RMSE is the square root of the variance, it can be interpreted as the standard deviation of what the observer can not describe. Errors will be presented in plots and analysed by studying the $RMSE$, calculation of $RMSE$ is defined by Equation 4.1.

$$\sqrt{\sum_{n=1}^{N} \frac{(y_{est}(n) - y_{meas}(n))^2}{N}}, \tag{4.1}$$

where N is the number of samples, y_{meas} the sensor measurements and y_{est} the estimates.

4.2.2   Estimation Error Histogram

The histogram of the estimation errors will be analysed in order to investigate the statistics of the estimation error $(y_{est}(n) - y_{meas}(n))$.

4.3   Validation Quantities

The Kalman filtered estimates will be validated against three different sensors, air mass flow W_c, air to fuel ratio λ, and EGR-fraction. The sensor for the air mass flow before the compressor W_c is considered the most accurate sensor and will therefore be used as the main validator. When an estimate is validated against a sensor the sensor data is not utilised in the calculations of the estimate, i.e. the sensor is not utilised for feedback in the EKF/UKF implementation.

4.3.1 λ (Air to Fuel Ratio)

The air to fuel ratio is defined by: $\lambda = \frac{(A/F)}{(A/F)_s}$ where A is the air mass flow into the engine, F the fuel mass flow into the engine and $(A/F)_s$ the stoichiometric air to fuel ratio which for diesel is 14.6. The ideal dataset to validate the estimate of λ against, would be λ from raw-sensor data of airmass flow (A) together with the given control input fuel mass flow and the stoichiometric air-to-fuel ratio. Unfortunately such data is seldom measured or logged due to the difficulties in measuring the airmass flow accurately. Instead the estimated λ will be validated against a partly modelled λ, described in Appendix B. Since high λ ($\lambda \gtrapprox 2$) does not lead to critical levels of smoke, it is more important to achieve good estimates when λ is low and the risk of smoke generation increase. When validating the estimates of λ the RMSE of λ^{-1} is used to better capture the errors of small λ, where the λ^{-1} estimates higher than 0.5 are of most interest. λ^{-1} is also know as the equivalence ratio ϕ and is shown in Figure 4.2.

4.3.2   EGR-fraction

EGR is a way to reduce NO_x by recirculating exhaust gas back into the engine cylinders. NO_x is created when oxygen and nitrogen reacts in the combustion chamber under high pressure and temperature. The exhaust gas will, when recirculated, act as an inert gas, (non-reactive gas), during the combustion and lower the combustion temperature, this makes it possible to reduce the NO_x substantially. A validation of EGR-fraction is done to see if the estimates can keep a good level when tuning the W_c estimate. Scanias virtual sensor of EGR-fraction from the validation data is presented in Figure 4.2 and the calculations of the estimated EGR in Appendix B.
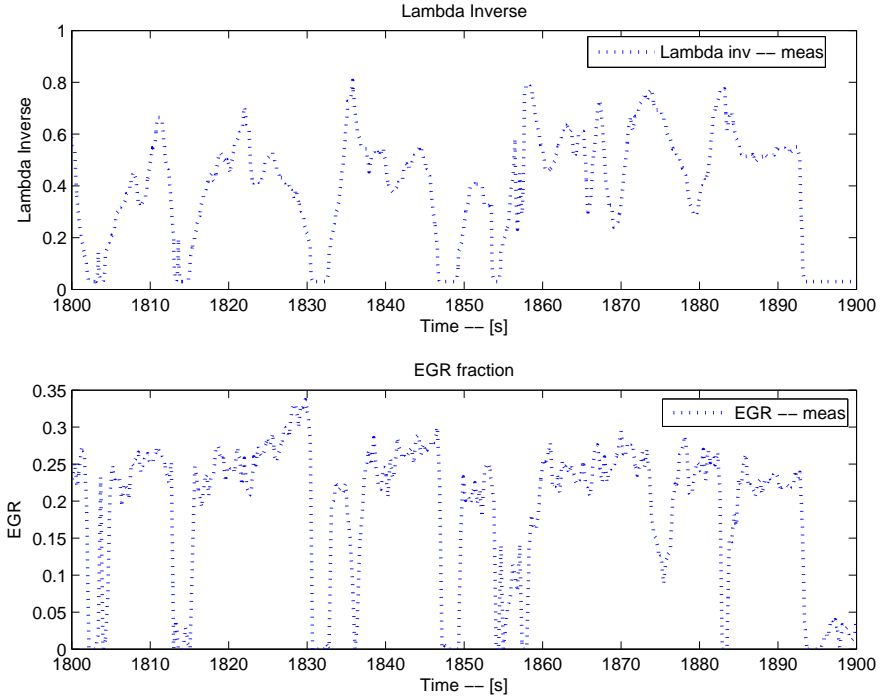
Figure 4.2. Plots of measured λ^{-1} and EGR-fraction

4.3.3 Air mass flow

Since the λ and EGR-fraction estimates are validated against virtual sensors, which are partly modelled, the validations are actually comparisons between different models. Another validation is therefore justified. W_c is the air mass flow before the compressor and is used to calculate the air mass flow into the engine (W_{ei}), which is used in calculations of λ and EGR- fraction, see Equation 4.2 and Equation 4.3. Since W_c is closely connected to λ and EGR-fraction and raw W_c sensor data is available, a validation between the estimated W_c and the measured W_c gives a better grading of the estimates. A plot of the measured W_c from the validation data can be seen in Figure 4.3

$$\lambda = \frac{W_{ei}X_{Oim}}{W_f(\frac{A}{F})_s X_{Oc}}, \tag{4.2}$$

$$x_{egr} = \frac{W_{egr}}{W_{ei}}, \tag{4.3}$$

For a full description of Equations 4.2 and 4.3 see Appendix B.
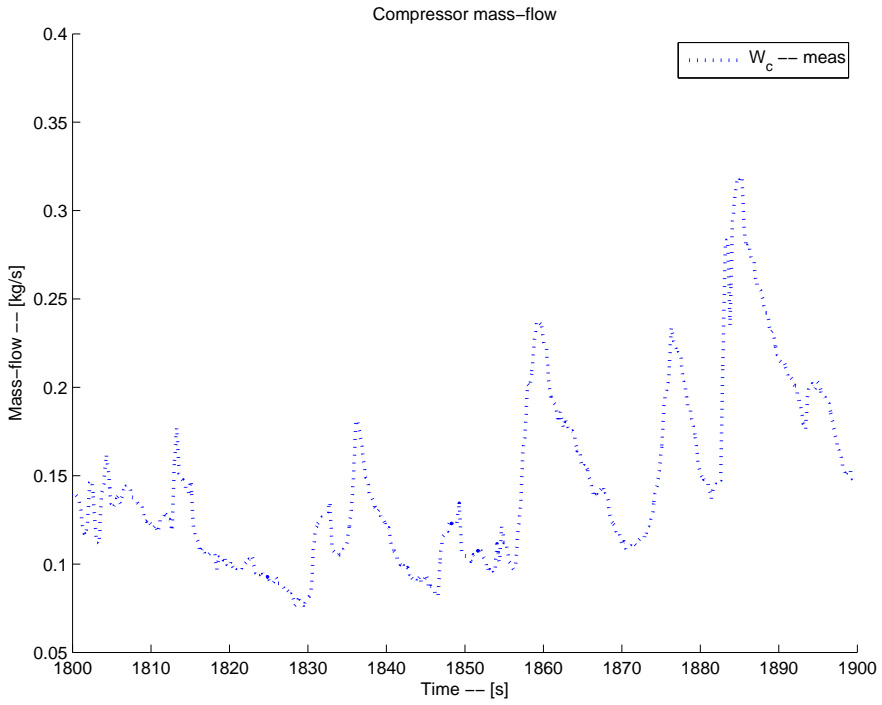
Figure 4.3. Plot of measured W_c.

Chapter 5

Model weaknesses

The Model output are analysed in this chapter as well as EKF estimates where the covariance of the measurement errors are set to values close to zero, i.e. a simulation with a high feedback gain from the measurements of p_{ic}, p_{im}, p_{em} and ω_t. The estimates from this EKF will be referred to as the high gain EKF estimates. An evaluation of the model output along with the high gain EKF estimates is presented in this Chapter using the validation methods in Chapter 4. The evaluation is performed with the intention to illuminate the weaknesses of the model and of completely trusting the measurements (high gain EKF) in order to show the necessity of Kalman filtering.

5.1   Model output of p_{ic}, p_{im}, p_{em} and ω_t

If simulating the model without taking feedback from measured signals into consideration, the estimates are poor. Estimates for p_{ic}, p_{im}, p_{em} and ω_t are compared to the corresponding measurements, see Figure 5.1. The estimates are only fairly good for short intervals, e.g. 1830-1835 s and around 1857 s, during these intervals EGR is low ($u_{egr} \lesssim 20\%$), the throttle is wide open ($u_{egr} = 100\%$), the injected fuel is low ($\delta \lesssim 75mg/str$) and the VGT is closed or partially opened ($u_{VGT} \lesssim 50\%$). The model has a hard time describing the dynamics of the system when the control signals are not in the mentioned intervals.
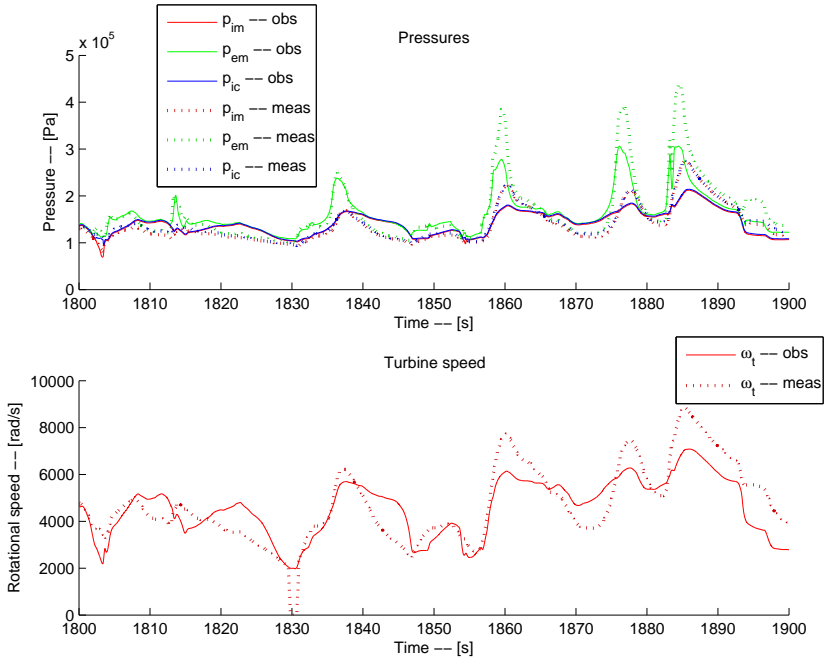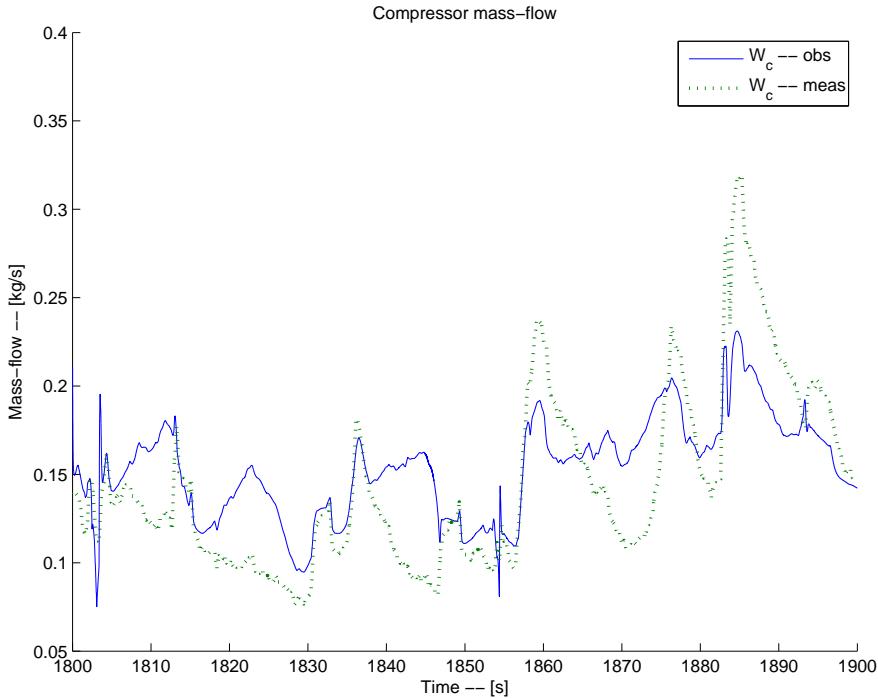
Figure 5.1. Plots of the model output of pressures and turbine speed.

Figure 5.2. Plots of model output of air mass flow W_c.
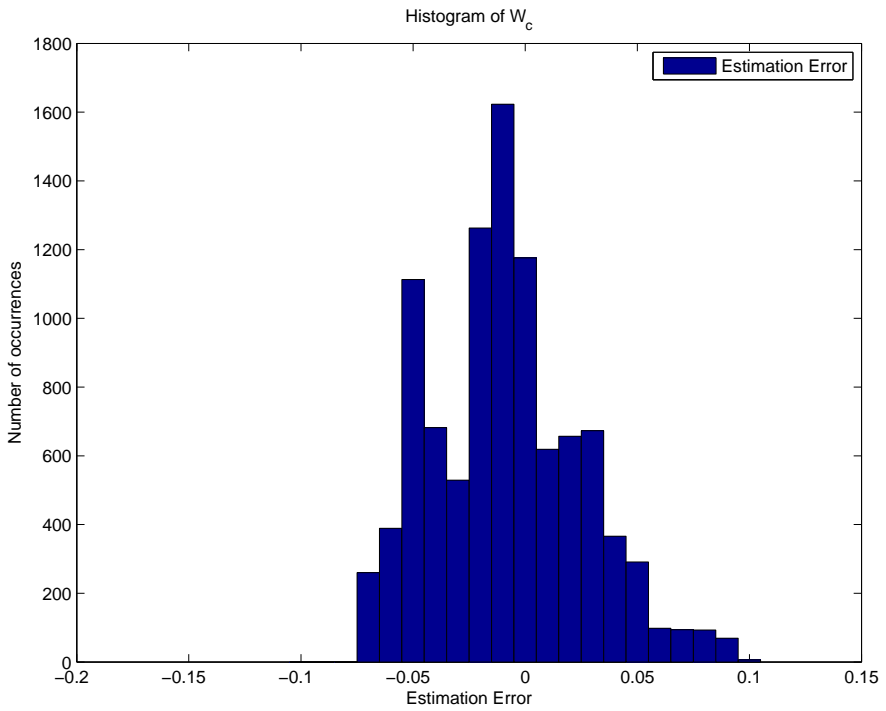
5.2 Model output of W_c

The W_c estimates are just as the other state estimates overall poor and only close to the measurements during short intervals, see Figure 5.2. The RMSE of W_c is shown in Table 5.1 and will later in this chapter be compared to RMSE for the Kalman filtered estimates of W_c.

5.3 Histogram of model output, W_c, estimation error

The histogram for W_c error in Figure 5.3 show that the two highest bars are placed in the negative error interval. This indicate that the estimates of W_c are often too big compared to the measurement. Since no clear Gaussian appearance are displayed its not just measurement noise that produce the errors but model errors contribute as well.

Table 5.1. RMSE of the model output

Error type	Simulation of model
RMSE for W_c	0.0347
RMSE for λ^{-1}	0.0981
RMSE for EGR	0.0914

Figure 5.3. Histogram of W_c-error calculated from model output.
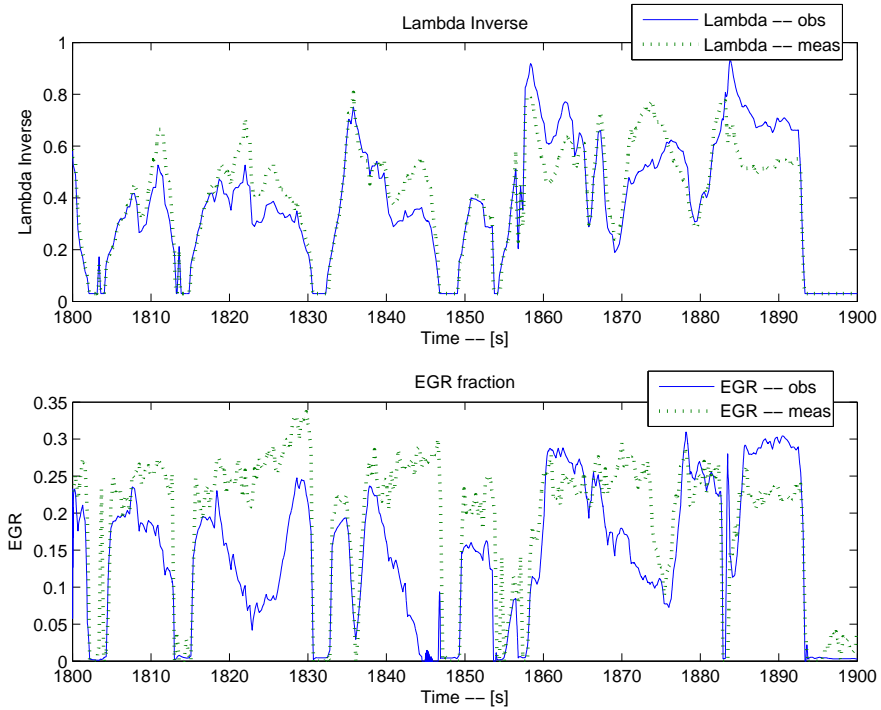
Figure 5.4. Plots of model output of λ^{-1} and *EGR*-fraction.

5.4   Model output of λ^{-1} and *EGR*- fraction

Since the state estimates are poor the λ^{-1} and EGR fraction end up with similar results because they are dependent of the states. The results are illustrated in Figure 5.4 and Table 5.1.
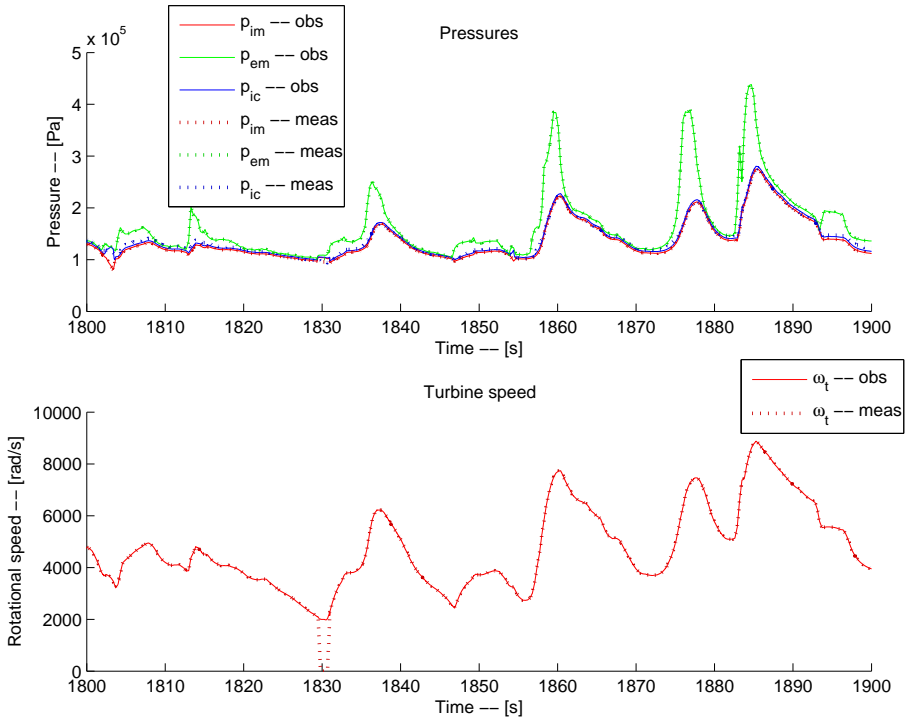
Figure 5.5. Plots of the high gain EKF estimates of pressures and turbine speed.

5.5   High gain EKF estimates of p_{ic}, p_{im}, p_{em} and ω_t.

Since measurements are highly prioritised here the estimates that correspond to the measured signals will be almost identical to the measured signals. This is also the case here and can be seen in Figure 5.5. The only time an estimate clearly deviates from its measured signal is for the ω_t around 1830 s. This is because the sensor can not measure signals under 2094 rad/sec, this was described in Section 3.4.
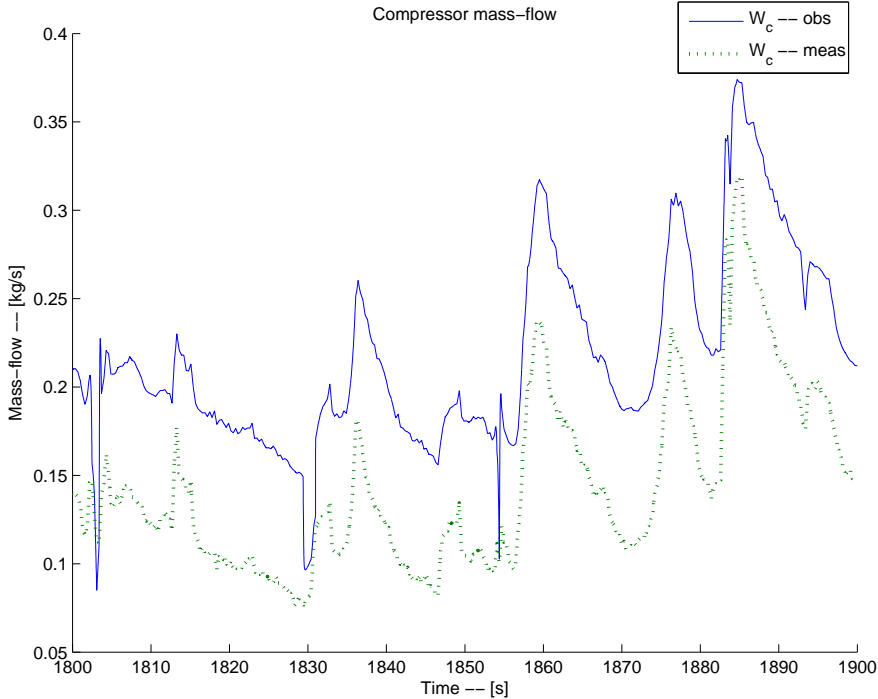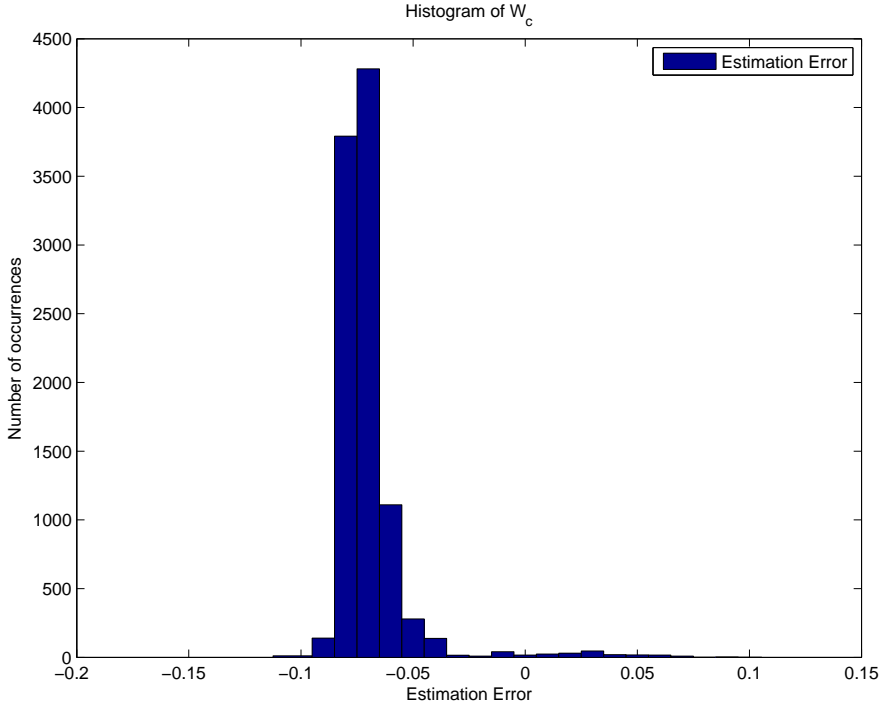
Figure 5.6. Plots of high gain EKF estimates of air mass flow W_c

5.6   High gain EKF estimates of W_c

Figure 5.6 and Table 5.2 show that the W_c estimates suffer considerably when trusting the measurements completely. The estimate of W_c is actually worse than the model estimates. Since the estimates in Section 5.5 follow the measurements well, the modelled transition from those states to W_c are not particularly good. Around 1830 s the W_c estimates are improved during a short interval, this is because the turbine speed is below 2094 rad/sec see Figure 5.5 and as explained in Section 3.4 trusting the model is chosen here due to stability issues. The fact that when trusting the model gives better estimates of W_c than when trusting the measurements at least for this short interval is interesting and will be used when tuning EKF/UKF later on. Around 1803 s and 1855 s fast throttle closing and opening occurs, see Figure 4.1, which result in improved high gain EKF estimates of W_c during the closing but when the throttle opens it exaggerates the W_c estimate and the offset proceeds.

Figure 5.7. Histogram of W_c error calculated from high gain EKF estimates

## 5.7 Histogram of high gain EKF, W_c, estimation error

The histogram of the W_c error based on measured p_{im}, p_{em}, p_{ic} and ω_t shows a left shifted and close to gaussian distribution, see Figure 5.7. This can be explained by the measurements ability to capture the dynamics and the offset shown in Figure 5.6.

5.8 High gain EKF estimates of λ^{-1} and EGR-fraction

Despite that the W_c estimate is worse than the model output of W_c, both the λ^{-1} and EGR-fraction estimates are improved compared to the model output, see Figure 5.8 and Table 5.2. This indicate that the model does a better job describing the transition from the measured states to λ^{-1} and EGR- fraction than it did for the W_c, which is of interest when adapting the EKF in Section 7.3.

Table 5.2. RMSE of the high gain EKF estimates

Error type	Simulation of model
RMSE for W_c	0.0739
RMSE for λ^{-1}	0.0361
RMSE for EGR	0.0652
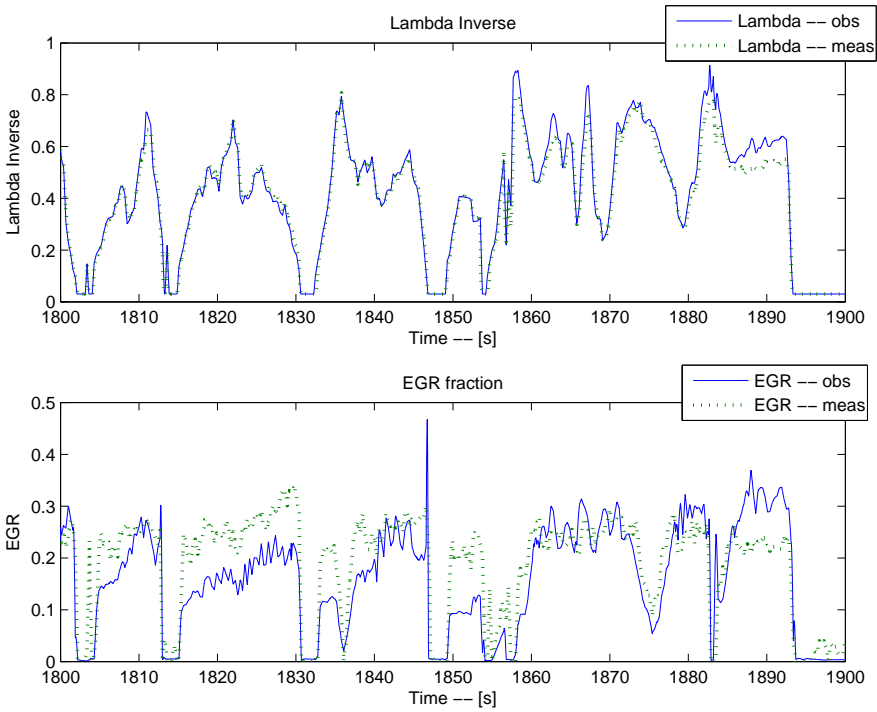
Figure 5.8. Plots of high gain EKF estimates of λ^{-1} and EGR-fraction.

5.9 Necessity of Kalman filtering

From this section it is established that the model output and the high gain EKF estimates are individually unable to describe the air mass flow before the compressor W_c. In Section 6 it is shown that together these two can improve the estimates significantly through Kalman filtering. Results from this chapter also reveal when the model and high gain EKF estimates are weak and therefore give input of how to adapt the filters in different operating points and how to divide these operating points into certain subsets, more about this in Chapter 7.

Chapter 6

Results: EKF vs UKF

The result from weighting the model output and system measurements through Kalman filtering will be reviewed in this chapter. EKF and UKF have different qualities and it will be determined which filter that can improve the estimates the most. Important factors in this filter comparison are accuracy in estimating W_c, computational complexity and robustness. The filters are tuned to give as good W_c estimates as possible but results for the other estimates are also of interest and therefore also presented in this Section.

6.1   EKF vs UKF: estimates of p_{ic}, p_{im}, p_{em} and ω_t

When using the EKF and UKF, feedback from measurements of p_{ic}, p_{im}, p_{em}, ω_t have been utilised as for the EKF in Section 5. The estimates from both EKF and UKF are close to the measurements but small offsets are allowed to improve the W_c estimates. Results of the EKF estimates are shown in Figure 6.1 and of the UKF estimates in Figure 6.2.

6.2   EKF vs UKF: stability and computational complexity

Table 6.1 shows that the EKF is more than twice as fast as the UKF when using the RK discretisation. This is because the UKF has to propagate all its sigma points through $f(x, u, n_e)$ in order to predict the states via the discretisation method (see Equation 3.13 in Chapter 3), which means that the UKF has to do as many predictions as it has sigma points in every time step, i.e. $4 * n_x + 1$ evaluations of $f(x, u, n_e)$. The EKF only has to do one prediction in every time step but have on the other hand demanding Jacobian calculations, requires $2 * n_x$ evaluations of $f(x, u, n_e)$. That the EKF is faster than the UKF is based on the amount of evaluations of $f(x, u, n_e)$ that has to be done, where the UKF has to do approximately twice as many as the EKF. The EKF manage to keep stability for larger time steps than the UKF see Table 6.1, this most likely originates from the fact
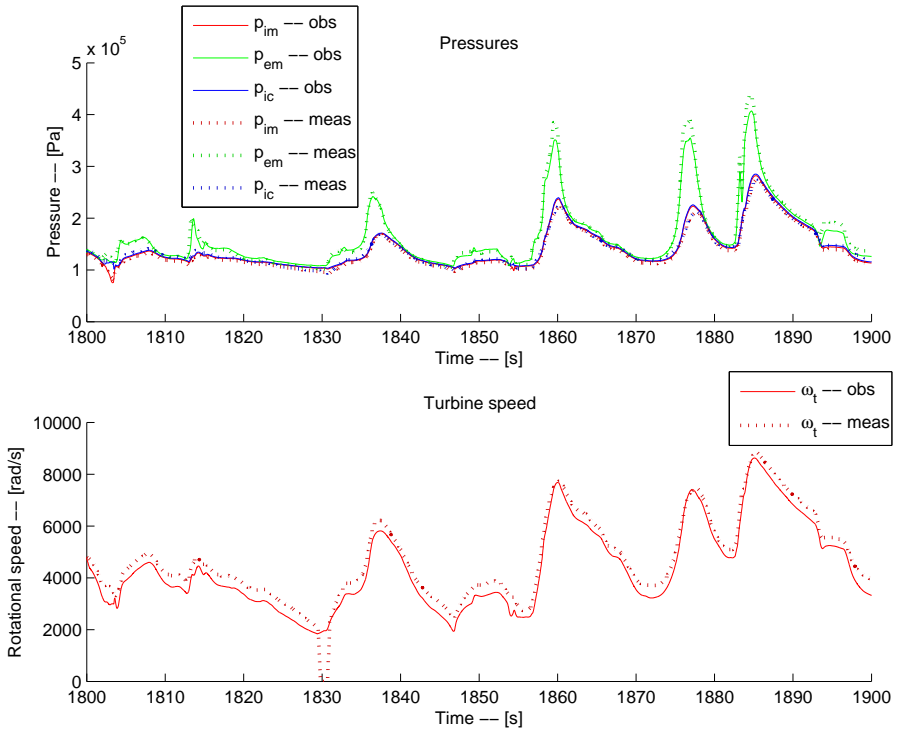
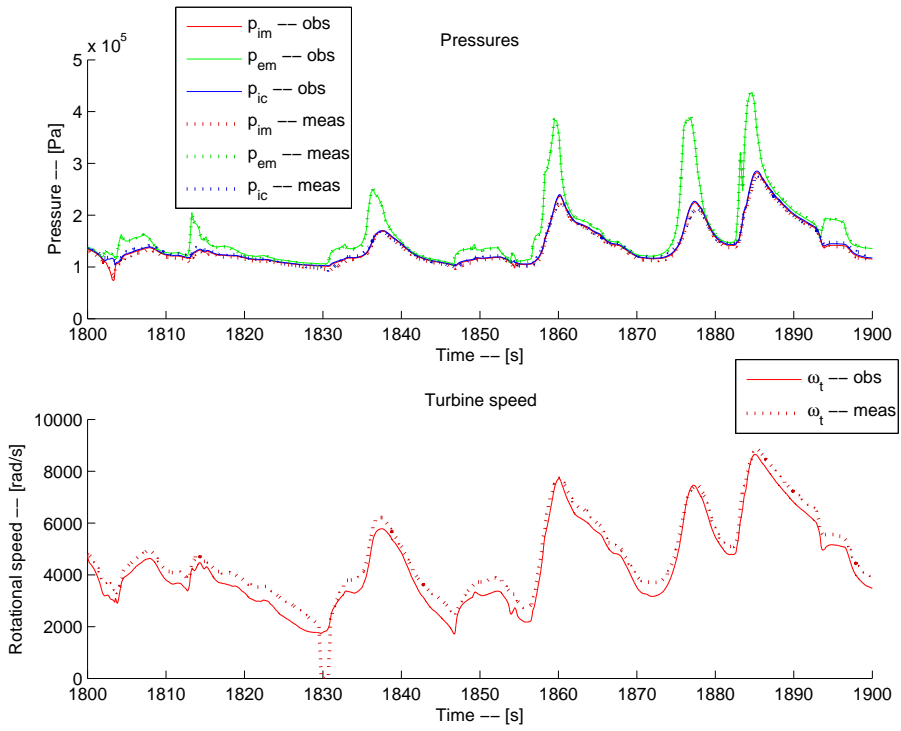**Figure 6.1.** Plots of the pressure and turbine speed estimates from EKF.

Figure 6.2. Plots of the pressure and turbine speed estimates from UKF.

Table 6.1. The upper test quantity is simulation time for interval 1800-1900 s with a sampling time of 0.01 s and the lower test quantity is sampling time when instability occurs for EKF and UKF using RK discretisation

Test quantity	EKF	UKF
Simulation time [s]	113.4	245.3
Instability sampling time [s]	0.030	0.012

Table 6.2. RMSE of W_c, λ^{-1} and *EGR*-fraction for EKF and UKF

Error type	EKF	UKF
RMSE for W_c	0.0110	0.0117
RMSE for λ^{-1}	0.0279	0.0348
RMSE for *EGR*	0.0380	0.0489

that the UKF uses the ODE model and the EKF uses the DAE model see 2.2. The presented results show that the EKF not only is faster, it is also more robust and therefore preferable during these circumstances.

6.3   EKF vs UKF: W_c estimates

The W_c estimates for the UKF and EKF are shown in Figure 6.3. The estimates are similar but the UKF usually estimate the peaks too high and the EKF a bit too low. Overall the EKF is closer to the measured W_c which also is revealed by the RMSE for the estimates illustrated in Table 6.2. If comparing the estimates from EKF and UKF with the earlier presented estimates from Section 5 a clear improvement for both EKF and UKF is seen.   The two histograms in Figures 6.4 and 6.5 show more Gaussian characteristics than the earlier histograms in Figures 5.3 and 5.7. The histograms are also located around the "zero" interval which demonstrate that the EKF and UKF provide estimates of W_c closer to the measured values and with a lower variance of the estimation error. The EKF have more errors in the negative error interval and the UKF have more errors in the positive error interval which indicate that the EKFs overall estimates are a bit to low and that the UKFs estimates are a bit to high.
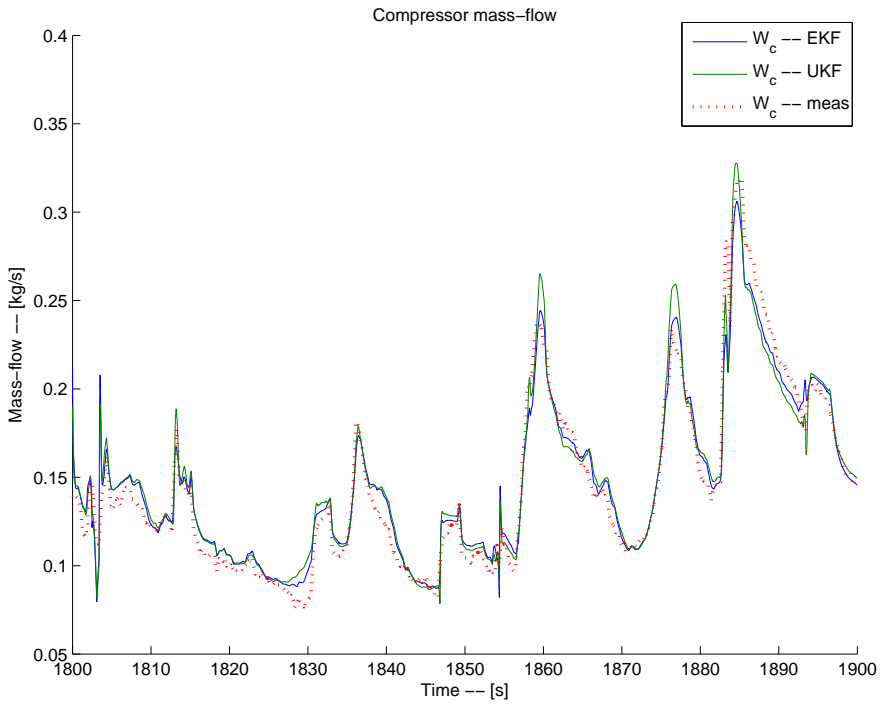
Figure 6.3. Plots of air mass flow W_c estimates from EKF and UKF.
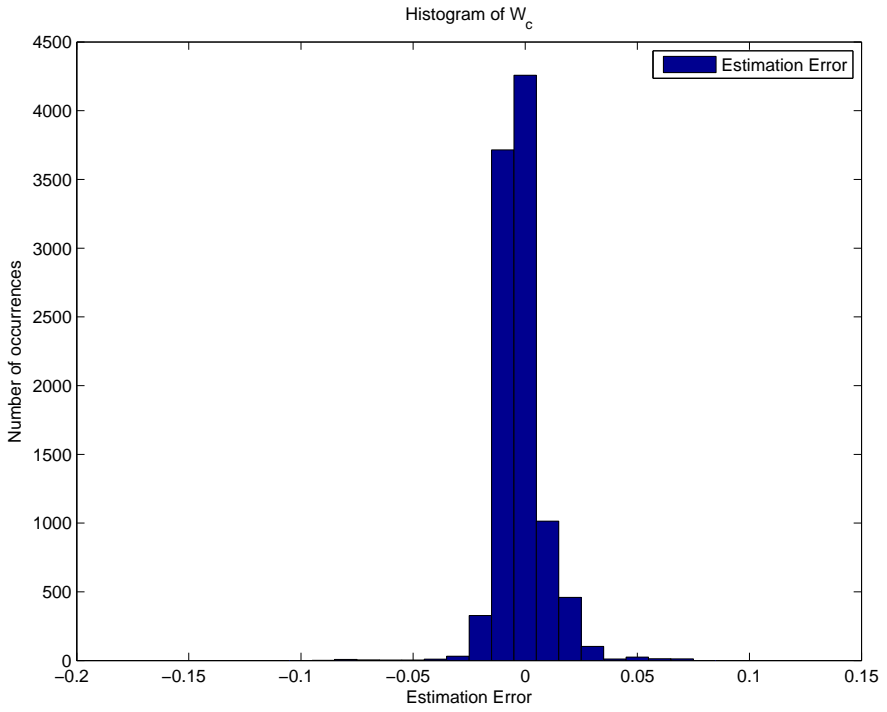
Figure 6.4. Histogram of W_c-error from EKF.
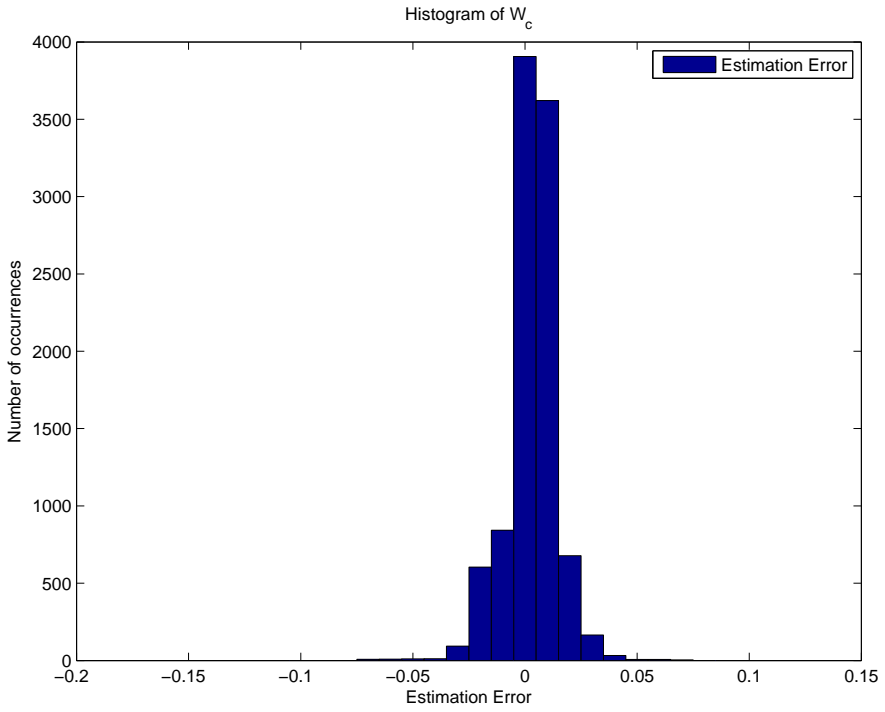
Figure 6.5. Histogram of W_c-error from UKF.

6.4 EKF vs UKF: Results for λ^{-1} and EGR fraction

For the λ^{-1} and EGR fraction estimates the UKF and EKF show similar results but the EKF is slightly better, compare Figure 6.7 with Figure 6.6 and see Table 6.2. Once again both UKF and EKF can display better estimates than the estimates presented in Section 5.
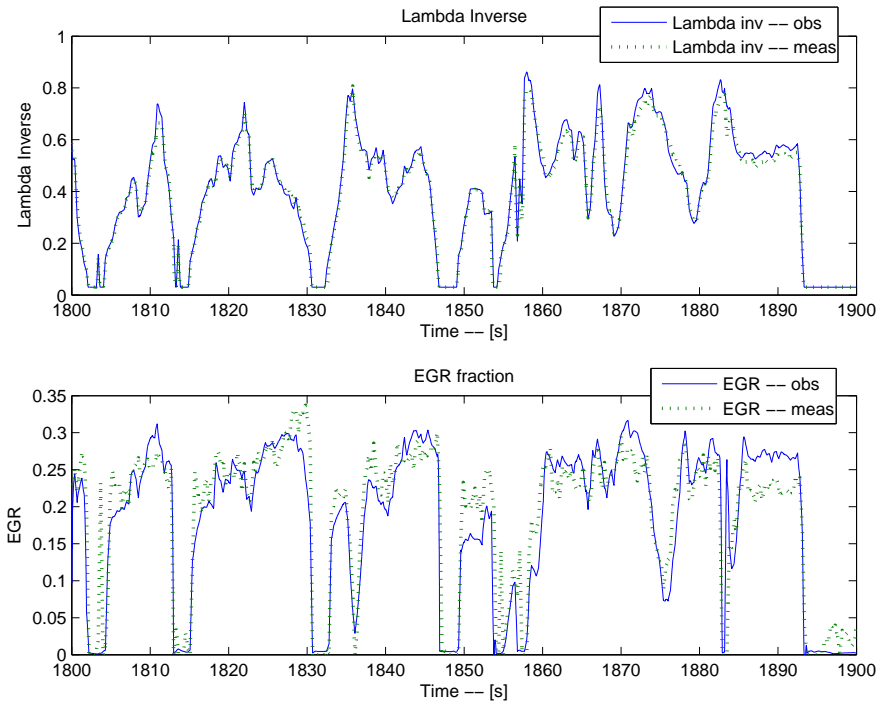
Figure 6.6. Plots of λ^{-1} and EGR-fraction estimates from EKF.
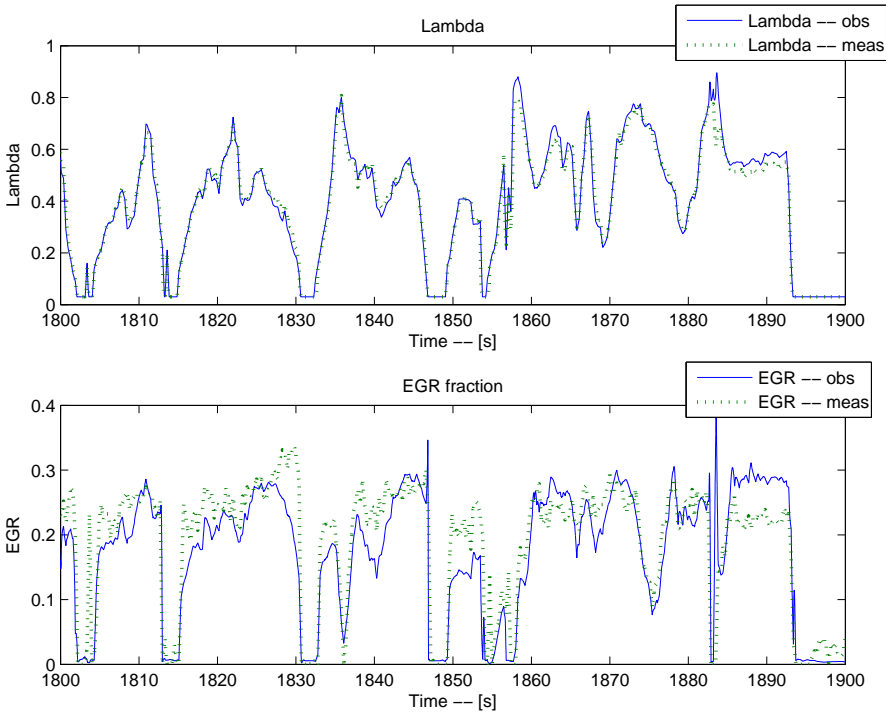
Figure 6.7. Plots of λ^{-1}, EGR-fraction estimates from UKF.

6.5   Kalman choise for adaptation

This chapter has revealed that the EKF is more appropriate for our model in almost every aspect, it is faster, gives better W_c estimates and is more stable than the UKF. The fact that the EKF is faster makes the tuning and adaptation easier since long simulation times are avoided. The stability issue is also of high importance for adaptation since changes of the noise covariances during simulation can make the estimates change quickly and therefore increase the risk of divergence. These reasons make the EKF preferable for adaptation and is therefore chosen to be augmented with an operating point dependent model and measurement noise, in Chapter 7.

Chapter 7

Adaptation of EKF

An adaptive filter can be obtained by choosing adaptive covariance matrices $Q(t)$ and $R(t)$ for the process and measurement noises w and e. Depending on the operating point, different $R(t)$ and $Q(t)$ are chosen that better describe the model and measurement quality under certain conditions. The relation between $R(t)$ and $Q(t)$ determines whether the measured signals or the model, should be trusted. By choosing the diagonal elements small for $R(t)$, i.e. small noise variances for the measured signals, the measured signals are considered accurate, while choosing them big implies the opposite. For $Q(t)$ the same reasoning is applied but for the model. Dividing all possible operating points to some subsets are necessary to make the adaptations possible.

7.1 Procedure

The use of EGR, VGT, injected fuel and Throttle has major impact on the model output and performance, therefore different combinations of these control signals have been chosen as subsets. Some control signals (VGT and EGR) are divided into two or even three subsets since the accuracy of the model output and high gain EKF estimates highly depend on the level of these control signals. The subsets are prioritised according to the order in Table 7.1, i.e. if two subsets are active, the one with the highest priority will be used. The subsets have been assigned their priority with consideration of the influence they have on the W_c estimates. The subsets are established through observing control signal intervals where the model output and/or high gain EKF estimates are poor, and trying to find control signal similarities during these intervals. In Figure 7.1 the control signals during a fast throttle opening is presented. In Figure 7.2 it is observed that high gain EKF estimates and model output diverge, a fast throttle opening is therefore an appropriate subset.
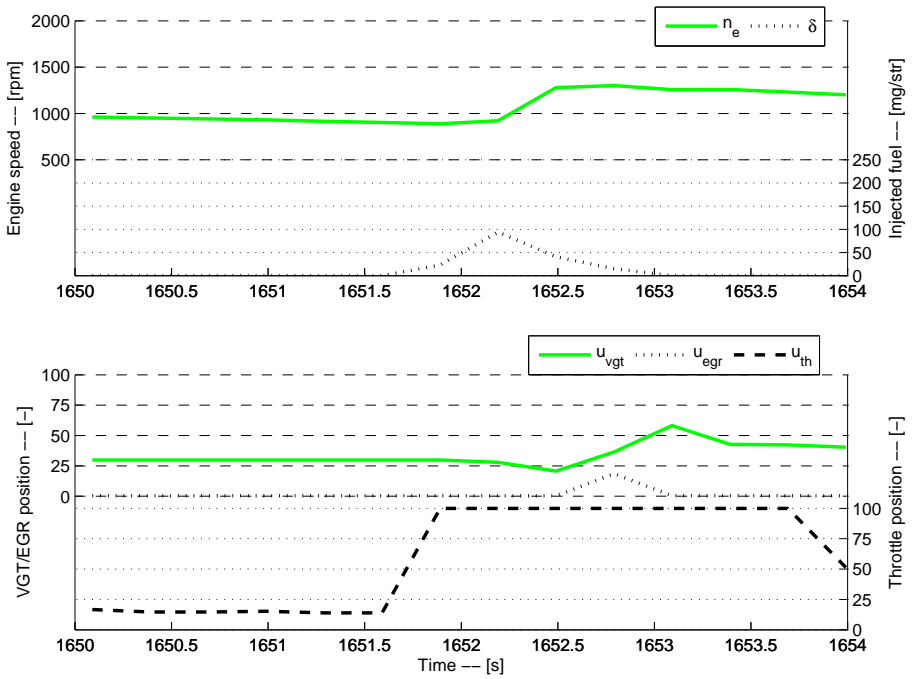
Figure 7.1. Plots of control signals during a fast throttle opening between 1651.5 s and 1652 s
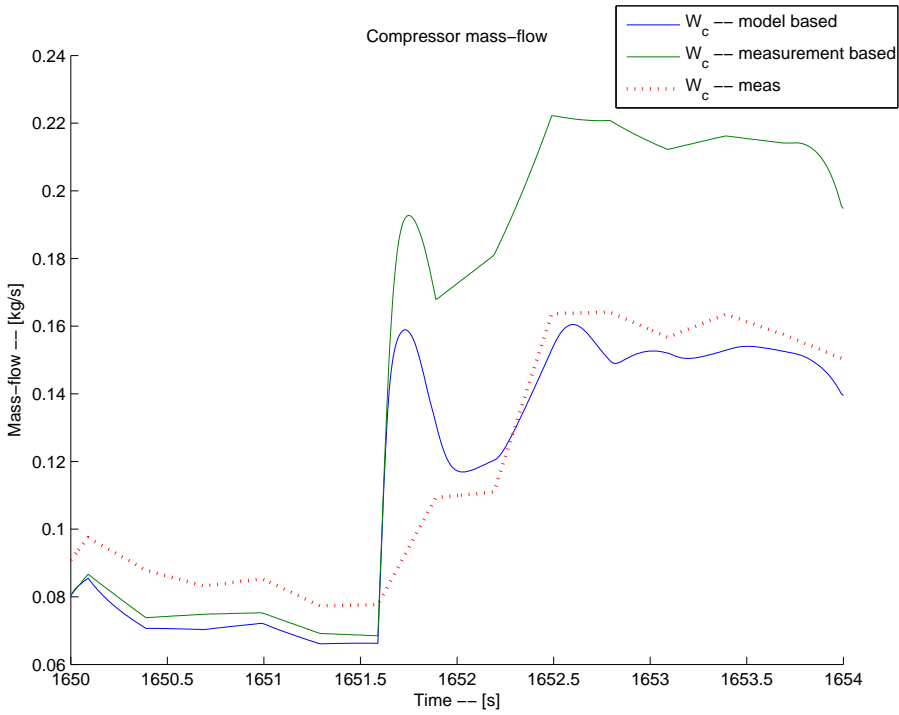
Figure 7.2. Plots of high gain EKF estimates and model output during a fast throttle opening.

The following subsets are used for the adaptive filtration.

Throttled subset Fast throttle opening (Throttle control signal derivative is larger than 100, $\frac{u_{th}(t)-u_{th}(t-1)}{T_s} > 100$).

High Fuel subset A lot of fuel is injected (Injected fuel is larger than 150 [mg/str], $\delta > 150$ [mg/str]).

EGR subset EGR is active but not too high (EGR- control signal: 75 % $\geq u_{egr}>$ 7 %).

High EGR subset EGR is active and high (EGR- control signal is: 95 % $\geq u_{egr}> 75$ %).

Top EGR subset EGR is active and very high (EGR- control signal is: $u_{egr} > 95$ %).

VGT subset VGT is partially opened (VGT- control signal is: $50 \geq u_{vgt} > 1$ %).

High VGT subset VGT is opened (VGT- control signal is: $u_{vgt} > 50$ %).

"Normal" subset None of the other subsets are active.

When the subsets are established, the next task is to choose proper $R(t)$ and $Q(t)$ for these subsets. As mentioned earlier Figure 7.2 shows a throttle subset, the throttle is opened fast, and as the plot illustrated the model output of W_c capture the changes better than the high gain EKF estimates which exaggerate the change in W_c. Hence a larger trust in the model is chosen during this subset, see $R1$ and $Q1$. The state that is closest connected W_c is ω_t which can be seen in Equation 7.1, and more detailed in Appendix B. It is therefore important to find good noise variances for the measurement and state prediction of ω_t and the tuning of ω_t:s noise variances has been highly valued. An example is if the ω_t estimate is close to the measured signal during the EGR subsets then the W_c estimate is poor. Not trusting the measured ω_t signal during EGR subsets is thus chosen.

$$W_c = \frac{p_{amb}\pi R_c^3 \omega_t \Phi_c}{(R_a T_{amb})} \tag{7.1}$$

Ways of determining suitable $R(t)$ and $Q(t)$ by observing model output and high gain EKF estimates are not always possible so a lot of the $R(t)$ and $Q(t)$ covariances are determined through trial and error. The adaptation covariances for different subsets are presented in Table 7.1 and the complete covariances are presented in Appendix A.

Table 7.1. Adaption settings

Subset	R- settings	Q-settings	Priority
Throttled	R1	Q1	1
High Fuel	R2	Q2	2
Top EGR	R3	Q3	3
High EGR	R4	Q4	4
EGR	R5	Q5	5
High VGT	R6	Q6	6
VGT	R7	Q7	7
Normal	R8	Q8	8

7.2   Smooth Transition

Hard transitions between subsets can cause unwanted jumps in the state estimates. A smoother transition between subsets has therefore been developed by making an interpolation between the current noise covariances R_t and Q_t and the requested noise covariances $R_{requested}$ and $Q_{requested}$. Figure 7.3 show the difference between using smooth transitions and not. Clear differences are seen around 1857[s] and 1858[s] where the smoother transition give a more desirable result. Algorithm 4 shows how a smooth transition is performed, one iteration is performed each time sample and the iterations will continue until a new subset of operating points is reached.

Algorithm 4: Smoothing Algorithm

---

1. If a transition between two subsets of operating points is made, set

$$
\begin{aligned}
Q_{Requested} &= Q_{NewSubset}, \\
R_{Requested} &= R_{NewSubset}.
\end{aligned}
$$

2. Calculate the difference between the present covariance matrices and the requested ones.

$$
\begin{aligned}
\triangle Q_t &= Q_{requested} - Q_{t-1}, \\
\triangle R_t &= R_{requested} - R_{t-1}.
\end{aligned}
$$

3. Update the covariance matrices.

$$
\begin{aligned}
Q_t &= Q_{t-1} + \frac{\triangle Q}{S_{factor}}, \\
R_t &= R_{t-1} + \frac{\triangle R}{S_{factor}},
\end{aligned}
$$

   where Q_t and R_t are the covariances used by the Kalman filter and the S_{factor} is the smoothing factor, set to 15 for this implementation, that will cause a smooth transition to the new covariance matrices.

4. Let $t := t + 1$ and if entering a new subset repeat from 1 else repeat from 2.
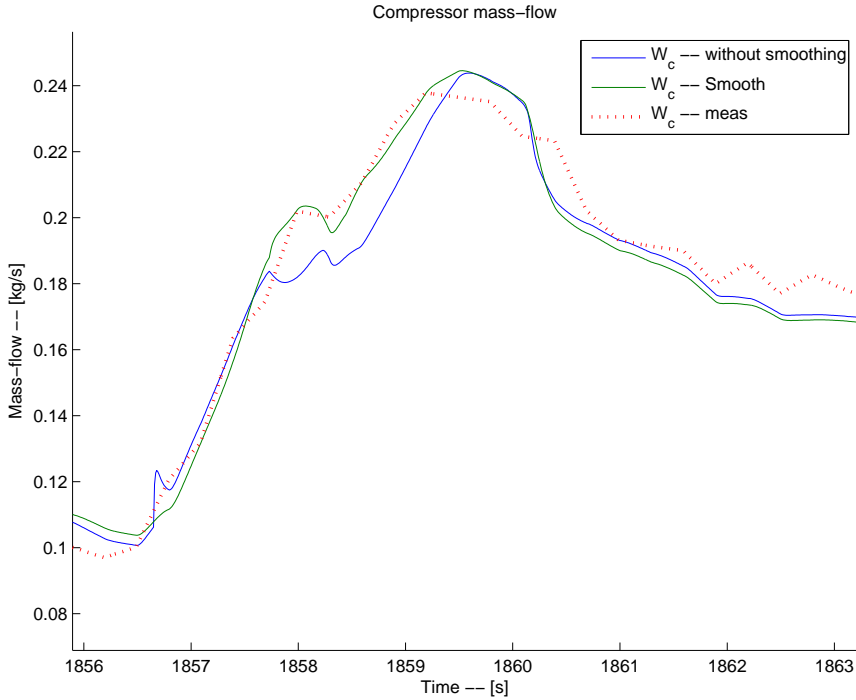

Figure 7.3. Plots of W_c estimates with and without smooth transition.

7.3   Results: Adaptive EKF

The efforts to improve the EKF by using adaptive covariances for measurement and model noise are presented in this section. A comparison to the regular EKF will be shown including improvements and error analysis.

7.3.1   Adaptive EKF estimates of p_{ic}, p_{im}, p_{em} and ω_t

The results of the measurable state estimates from the adaptive EKF are illustrated in Figure 7.4. The estimates are similar to the ones from the EKF in Figure 6.1 but with the difference that the turbine speed (ω_t) differ from the measured signal more clearly for some intervals. During these intervals a lot of EGR is used, see control signals in Figure 4.1. A turbine speed estimate (ω_t) close to the measured signal during a lot of EGR tends to give bad air mass flow estimates (W_c). The Adaptive EKF compensate for high EGR by not trusting the measured turbine speed in these intervals, hence the inadequacy in turbine speed estimates.
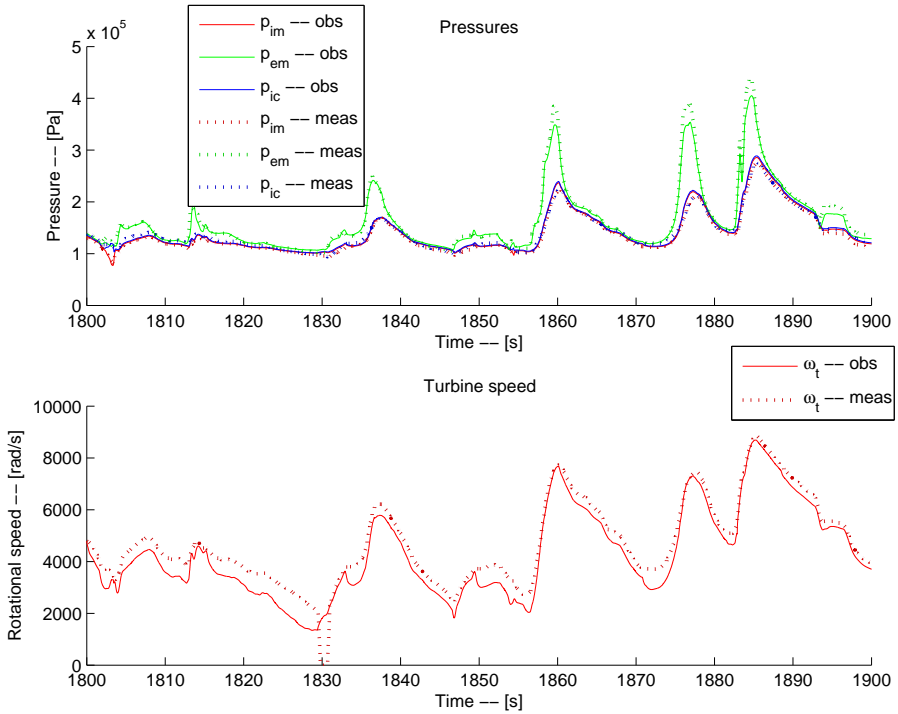
Figure 7.4. Plots of the pressures and engine speed from Adaptiv EKF.

7.3.2   Adaptive EKF estimates of W_c

By judging from Figure 7.5 and Table 7.2 the Adaptiv EKF manage to estimate W_c better than the EKF. If comparing the Adaptive EKF and the EKF, a decrease with approximately 23 % in RMSE is shown while using the Classical Runge Kutta method. The adaptive EKF gets its biggest benefits during high fuel injections which can be seen around the three highest peaks in Figure 7.5 compared to the corresponding peaks in Figure 6.3. The reason for this distinction is that the "regular" EKF has to prioritise the most common subsets of operating points in order to get as good overall estimates as possible. The Adaptive EKF on the other hand does not have that limitation and can adapt for the not so common subsets of operating points.

Table 7.2. RMSE comparison of EKF and Adaptive EKF.

Model	Model output	High gain EKF	EKF	Adaptiv EKF
RMSE for W_c	0.0347	0.0739	0.0110	0.0085
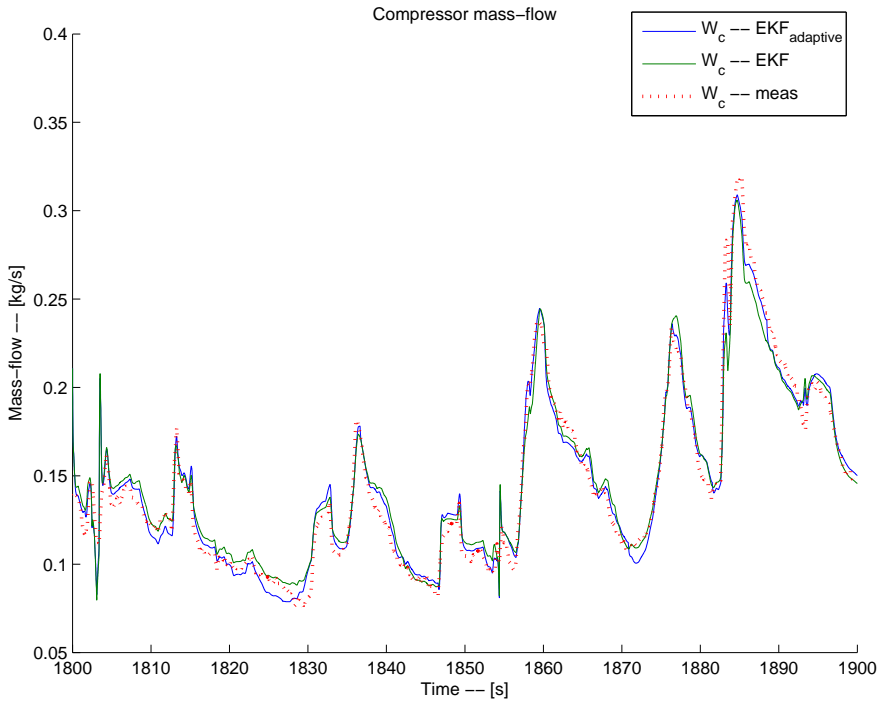
**Figure 7.5.** Plots of air mass flow from EKF and Adaptiv EKF.

7.3.3   Histogram of W_c estimation error

The error for estimated W_c is illustrated in a histogram in Figure 7.6. A clear peak is located around the zero error interval with about evenly high bars next to it, which point out a low error for W_c whitout offsets and an improvement in comparison to the estimation error of the regular EKF.

Table 7.3. RMSE of λ^{-1} and *EGR*-fraction from Adaptive EKF

Error type	Model output	High gain EKF	EKF	Adaptive EKF
RMSE for λ^{-1}	0.0981	0.0361	0.0279	0.0381
RMSE for *EGR*	0.0914	0.0652	0.0380	0.0403
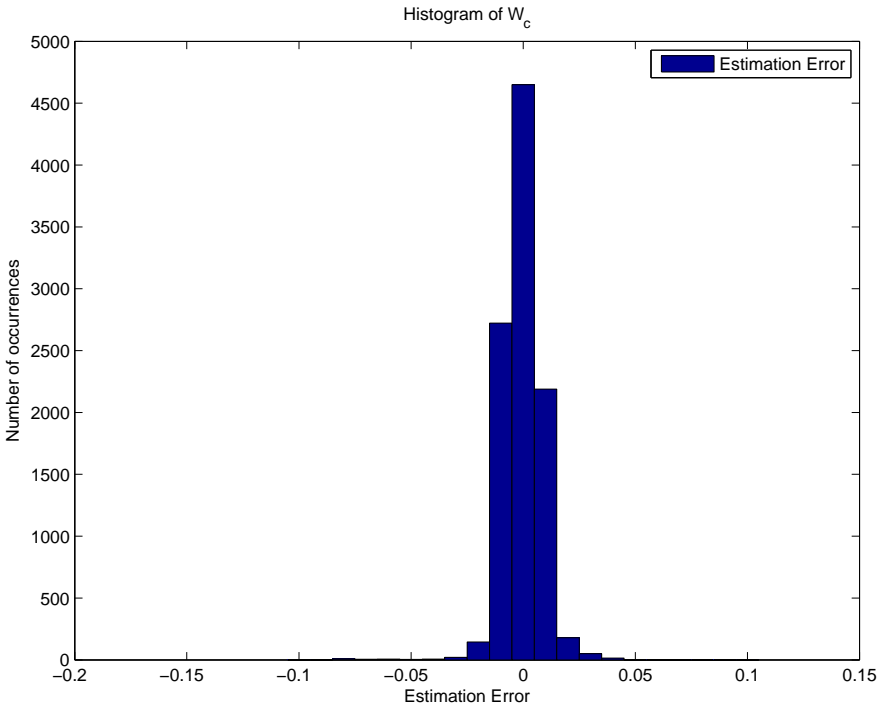
Figure 7.6. Histogram of W_c-error from adaptive EKF.

7.3.4 Adaptive EKF estimates of λ^{-1} and EGR fraction

The EKF is adapted to trust the model in some operating points to be able to improve the estimates of W_c. Unfortunately this result in worse estimates for λ^{-1} and EGR- fraction, since the model fail in describing those. To see the differences between EKF and Adaptive EKF, see Table 7.3 and compare Figure 7.7 with Figure 6.6.
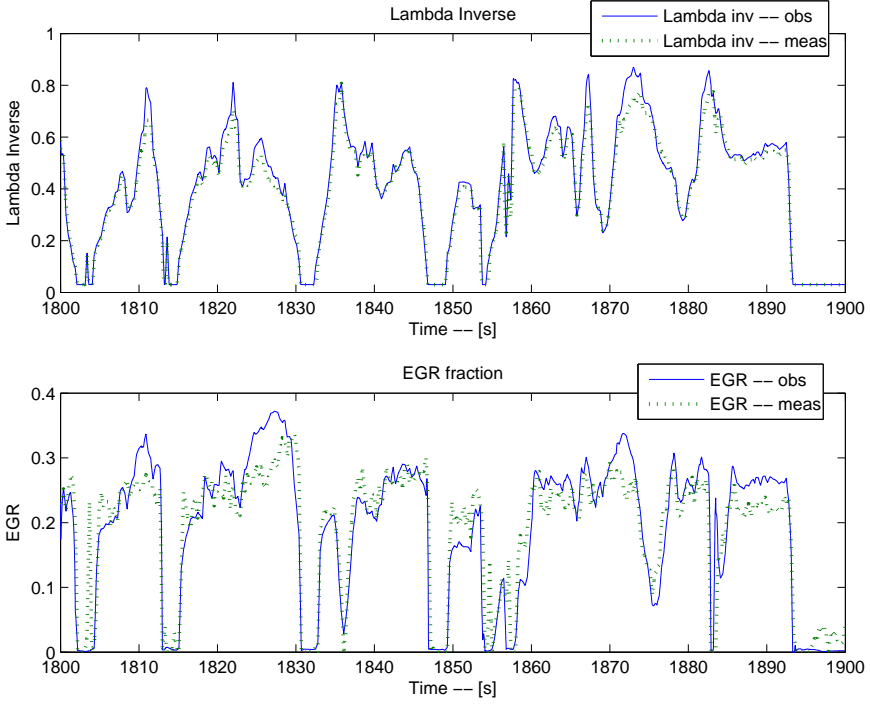
Figure 7.7. Plots of λ^{-1} and EGR-fraction estimates from Adaptive EKF.

Chapter 8

Conclusions and Future Research

8.1 Conclusions

Estimates from a diesel engine model with intake throttle, VGT and EGR are improved with help from Kalman filtering, sensors and advanced mathematics. The improvements are made to investigate the possibility of replacing existing sensors to cut cost or to acquire additional information for state accuracy. The improved estimates for the air to fuel ratio λ, Exhaust Gas Recirculation (EGR-fraction) and air mass flow before the compressor W_c are compared to existing sensors. The W_c-sensor is considered most accurate and used for validation. A comparison between the EKF and UKF is made and the UKF is unable to match the results of the EKF. The EKF is improved further to an Adaptive Extended Kalman Filter which is proven to give better results than the regular EKF. The W_c sensor can be replaced by the Adaptive Extended Kalman Filter estimates with a Root Mean Square Error (RMSE) of 0.0085 kg/s. The W_c estimates are used when estimating λ and EGR-fraction which result in a RMSE of 0.0403 for the EGR-fraction and 0.0381 for λ^{-1}, (λ^{-1} is used to capture the more important errors when λ is less than 2). The estimates can also be used as a replacement in case of sensor failure.

8.2 Future Research

Both the ODE and the DAE engine model have advantages, the ODE describe the dynamics of the intercooler pressure better especially during throttle changes and the DAE tends to give a more robust system while using it in a Kalman Filter. A Kalman Filter that switches between these models would therefore be interesting. A risk is that when switching between models the state estimates might jump which will be a challenge to avoid.
If having knowledge about the sensors that are used a tuning based on that knowl-

edge can be used for the R covariance matrix (covariance for measurement noise). If also knowing how the accuracy of the sensors change over time an adaptation of the R matrix can be used to be able too maintain good estimates although the sensor data fail in accuracy. Another aspect could be if the diagnosis system in the engine gave input to the Kalman Filter so it could adapt its R and Q matrices dependant of that information.

Research have been done to implement a hybrid Kalman Filter consisting of UKF and EKF [4] called UEKF. The effort is made too reduce the long simulation times for the UKF but still maintain some of the good qualities from the UKF. The UEKF use the regular measurement update from the EKF, i.e. it estimates mean and covariances of the states just as the EKF does during measurement update. In the time update however the UEKF use the Unscented Transform and predict the new states just as the UKF does. The covariance is predicted by using linearisation (from EKF) on all sigma points (from UKF) and then calculating a mean value of those. Trying this UEKF for the engine model used in this report could be an interesting investigation.

EKF based on the DAE model has shown improvements to the EKF based on the ODE model, see Section 2.2. Implementing an UKF based on that DAE model instead of the ODE model, that is used in this report, would therefore be an interesting continuation.

Bibliography

[1] Wan E. A. and Van Der Merwe R. The unscented kalman filter for nonlinear estimation. 2002.

[2] F. Scortecci A. Giannitrapani, N. Ceccarelli and A. Garulli. Comparison of ekf and ukf for spacecraft localization via angle measurements. 2011.

[3] M. Ahmad and M. Chang. Comparison of the simple ekf, iekf, and ukf for a sensorless full-digital pmsm drive. 2005.

[4] Penglang Shui Changyun Liu and Song Li. Unscented extended kalman filter for target tracking. 2011.

[5] Analysis Factor. Rmse. http://www.analysisfactor.com/statchat/?tag=rmse, 2008.

[6] G.Hendeby. Performance and implementation aspects of nonlinear filtering, 2008.

[7] Fredrik Gustafsson. *Statistical Sensor Fusion.* Studentlitteratur, 2010.

[8] Erik Höckerdal, Erik Frisk, and Lars Eriksson. Dae and ode based ekf:s and their real-time performance evaluated on a diesel engine. 2011.

[9] Julier S. J., Uhlmann J. K., and Durrant-Whyte H. F. A new approach for filtering nonlinear systems, 1995.

[10] Simon J. Julier and Jeffrey K. Uhlmann. Unscented filtering and nonlinear estimation, 2004.

[11] R. E. Kalman. A new approach to linear filtering and prediction problems. 1960.

[12] R Kumar Mandela, Raghunathan Rengaswamy, and Shankar Narasimhan. Recursive state estimation techniques for nonlinear differential algebraic systems. *Chemical Engineering Science*, 65:4548–4556, 2010.

[13] Rudolph Van Der Merwe and Eric Wan. Sigma-point kalman filters for integrated navigation, 2004.

[14] Diesel Net. Whtc. http://www.dieselnet.com/standards/cycles/whtc.php, 2011.

[15] L Nielsen and L Eriksson. Vehicular systems, 2007.

[16] B. Hassibi T. Kailath, A.H. Sayed. *Linear Estimation*. Prentice Hall, 2000.

[17] G W Griffiths V M Becerra, P D Roberts. Applying the extended kalman filter to systems described by nonlinear differential-algebraic equations. control engineering practice, 2001.

[18] Johan Wahlström and Lars Eriksson. Modeling of a diesel engine with intake throttle, VGT, and EGR. Technical Report LiTH-R-2976, Department of Electrical Engineering, Linköpings Universitet, SE-581 83 Linköping, Sweden, 2010.

Appendix A

Covariance Matrices

The adapted R and Q matrices are: R1,...,R8 and Q1,...,Q8

$$R1 = 10^7 * \begin{pmatrix} 0.00001 & 0 & 0 & 0 \\ 0 & 0.00001 & 0 & 0 \\ 0 & 0 & 1 & 0 \\ 0 & 0 & 0 & 0.01 \end{pmatrix} \tag{A.1}$$

$$Q1 = 10^{-7} * \begin{pmatrix} 0.00001 & 0 & 0 & 0 & 0 & 0 \\ 0 & 0.000000000001 & 0 & 0 & 0 & 0 \\ 0 & 0 & 0.000000000001 & 0 & 0 & 0 \\ 0 & 0 & 0 & 0.0000000001 & 0 & 0 \\ 0 & 0 & 0 & 0 & 0.5 & 0 \\ 0 & 0 & 0 & 0 & 0 & 0.1 \end{pmatrix} \tag{A.2}$$

$$R2 = 10^8 * \begin{pmatrix} 0.000001 & 0 & 0 & 0 \\ 0 & 0.000001 & 0 & 0 \\ 0 & 0 & 0.00000001 & 0 \\ 0 & 0 & 0 & 1 \end{pmatrix} \tag{A.3}$$

$$Q2 = \begin{pmatrix} 0.0000005 & 0 & 0 & 0 & 0 & 0 \\ 0 & 0.00000000000005 & 0 & 0 & 0 & 0 \\ 0 & 0 & 0.00000000000005 & 0 & 0 & 0 \\ 0 & 0 & 0 & 0.00125 & 0 & 0 \\ 0 & 0 & 0 & 0 & 0.005 & 0 \\ 0 & 0 & 0 & 0 & 0 & 0.005 \end{pmatrix} \tag{A.4}$$

$$R3 = 10^5 * \begin{pmatrix} 0.0010 & 0 & 0 & 0 \\ 0 & 0.0010 & 0 & 0 \\ 0 & 0 & 0.000007 & 0 \\ 0 & 0 & 0 & 1 \end{pmatrix} \tag{A.5}$$

$$Q3 = \begin{pmatrix} 0.000001 & 0 & 0 & 0 & 0 & 0 \\ 0 & 0.0000000000001 & 0 & 0 & 0 & 0 \\ 0 & 0 & 0.0000000000001 & 0 & 0 & 0 \\ 0 & 0 & 0 & 0.0025 & 0 & 0 \\ 0 & 0 & 0 & 0 & 0.01 & 0 \\ 0 & 0 & 0 & 0 & 0 & 0.01 \end{pmatrix} \tag{A.6}$$

$$R4 = 10^8 * \begin{pmatrix} 0.000001 & 0 & 0 & 0 \\ 0 & 0.000001 & 0 & 0 \\ 0 & 0 & 0.00000001 & 0 \\ 0 & 0 & 0 & 1 \end{pmatrix} \tag{A.7}$$

$$Q4 = \begin{pmatrix} 0.000001 & 0 & 0 & 0 & 0 & 0 \\ 0 & 0.0000000000001 & 0 & 0 & 0 & 0 \\ 0 & 0 & 0.0000000000001 & 0 & 0 & 0 \\ 0 & 0 & 0 & 0.0025 & 0 & 0 \\ 0 & 0 & 0 & 0 & 0.01 & 0 \\ 0 & 0 & 0 & 0 & 0 & 0.01 \end{pmatrix} \tag{A.8}$$

$$R5 = 10^8 * \begin{pmatrix} 0.000001 & 0 & 0 & 0 \\ 0 & 0.000001 & 0 & 0 \\ 0 & 0 & 0.000001 & 0 \\ 0 & 0 & 0 & 1 \end{pmatrix} \tag{A.9}$$

$$Q5 = \begin{pmatrix} 0.000001 & 0 & 0 & 0 & 0 & 0 \\ 0 & 0.0000000000001 & 0 & 0 & 0 & 0 \\ 0 & 0 & 0.0000000000001 & 0 & 0 & 0 \\ 0 & 0 & 0 & 0.005 & 0 & 0 \\ 0 & 0 & 0 & 0 & 0.01 & 0 \\ 0 & 0 & 0 & 0 & 0 & 0.01 \end{pmatrix} \tag{A.10}$$

$$R6 = 10^9 * \begin{pmatrix} 0.0000001 & 0 & 0 & 0 \\ 0 & 0.0000001 & 0 & 0 \\ 0 & 0 & 0.0000000001 & 0 \\ 0 & 0 & 0 & 1 \end{pmatrix} \qquad (A.11)$$

$$Q6 = \begin{pmatrix} 0.0000001 & 0 & 0 & 0 & 0 & 0 \\ 0 & 0.0000000000001 & 0 & 0 & 0 & 0 \\ 0 & 0 & 0.0000000000001 & 0 & 0 & 0 \\ 0 & 0 & 0 & 0.001 & 0 & 0 \\ 0 & 0 & 0 & 0 & 0.01 & 0 \\ 0 & 0 & 0 & 0 & 0 & 0.0001 \end{pmatrix}$$
$$(A.12)$$

$$R7 = 10^9 * \begin{pmatrix} 0.0000001 & 0 & 0 & 0 \\ 0 & 0.0000001 & 0 & 0 \\ 0 & 0 & 0.0000000001 & 0 \\ 0 & 0 & 0 & 1 \end{pmatrix} \qquad (A.13)$$

$$Q7 = \begin{pmatrix} 0.0000001 & 0 & 0 & 0 & 0 & 0 \\ 0 & 0.0000000000001 & 0 & 0 & 0 & 0 \\ 0 & 0 & 0.0000000000001 & 0 & 0 & 0 \\ 0 & 0 & 0 & 0.001 & 0 & 0 \\ 0 & 0 & 0 & 0 & 0.01 & 0 \\ 0 & 0 & 0 & 0 & 0 & 0.0001 \end{pmatrix}$$
$$(A.14)$$

$$R8 = 10^5 * \begin{pmatrix} 0.001 & 0 & 0 & 0 \\ 0 & 0.001 & 0 & 0 \\ 0 & 0 & 0.00001 & 0 \\ 0 & 0 & 0 & 1 \end{pmatrix} \qquad (A.15)$$

$$Q8 = \begin{pmatrix} 0.000001 & 0 & 0 & 0 & 0 & 0 \\ 0 & 0.0000000000001 & 0 & 0 & 0 & 0 \\ 0 & 0 & 0.0000000000001 & 0 & 0 & 0 \\ 0 & 0 & 0 & 0.001 & 0 & 0 \\ 0 & 0 & 0 & 0 & 0.01 & 0 \\ 0 & 0 & 0 & 0 & 0 & 0.01 \end{pmatrix}$$
$$(A.16)$$

Q and R matrices for UKF.

$$
R = \begin{pmatrix} 100 & 0 & 0 & 0 \\ 0 & 100 & 0 & 0 \\ 0 & 0 & 1 & 0 \\ 0 & 0 & 0 & 100 \end{pmatrix} \tag{A.17}
$$

$$
Q = \begin{pmatrix} 0.000001 & 0 & 0 & 0 & 0 & 0 & 0 \\ 0 & 0.0000000000001 & 0 & 0 & 0 & 0 & 0 \\ 0 & 0 & 0.0000000000001 & 0 & 0 & 0 & 0 \\ 0 & 0 & 0 & 0.001 & 0 & 0 & 0 \\ 0 & 0 & 0 & 0 & 0.01 & 0 & 0 \\ 0 & 0 & 0 & 0 & 0 & 0.01 & 0 \\ 0 & 0 & 0 & 0 & 0 & 0 & 0.01 \end{pmatrix} \tag{A.18}
$$

Appendix B

Model

Manifolds

INTAKE MANIFOLD

$$\frac{d}{dt}p_{\text{im}} = \frac{R_{\text{a}} T_{\text{im}}}{V_{\text{im}}} \left(W_{\text{th}} + W_{\text{egr}} - W_{\text{ei}}\right)$$

EXHAUST MANIFOLD

$$\frac{d}{dt}p_{\text{em}} = \frac{R_{\text{e}} T_{\text{em}}}{V_{\text{em}}} (W_{\text{eo}} - W_{\text{egr}} - W_{\text{t}}) + \frac{p_{\text{em}}}{T_{\text{em}}} \frac{d}{dt} T_{\text{em}}$$

$$\frac{d}{dt}T_{\text{em}} = \frac{R_{\text{e}} T_{\text{em}}}{p_{\text{em}} V_{\text{em}} c_{\text{ve}}} \big((W_{\text{eo}} - W_{\text{egr}} - W_{\text{t}}) \, c_{\text{ve}}(T_{\text{em,in}} - T_{\text{em}}) +$$
$$R_{\text{e}}(T_{\text{em,in}} \, (W_{\text{eo}} - W_{\text{egr}} - W_{\text{t}}) - T_{\text{em}} \, (-W_{\text{eo}} + W_{\text{egr}} + W_{\text{t}})))$$

INTERCOOLER

$$\frac{d}{dt}p_{\text{ic}} = \frac{R_{\text{a}} T_{\text{im}}}{V_{\text{ic}}} \left(W_{\text{c}} - W_{\text{th}}\right)$$

$$x_{\text{egr}} = \frac{W_{\text{egr}}}{W_{\text{th}} + W_{\text{egr}}}$$

Intake manifold

$$\frac{d}{dt}X_{\text{Oim}} = \frac{R_{\text{a}} T_{\text{im}}}{p_{\text{im}} V_{\text{im}}} \big((X_{\text{Oc}} - X_{\text{Oim}}) \max(W_{\text{th}}, 0) + (X_{\text{Oem}} - X_{\text{Oim}}) \max(W_{\text{egr}}, 0)$$
$$- X_{\text{Oim}} \max(-W_{\text{ei}}, 0)\big)$$

Exhaust manifold

$$\frac{d}{dt}X_{\text{Oem}} = \frac{R_{\text{e}} T_{\text{em}}}{p_{\text{em}} V_{\text{em}}} \big((X_{\text{Oe}} - X_{\text{Oem}}) \max(W_{\text{eo}}, 0) + (X_{\text{Oim}} - X_{\text{Oem}}) \max(-W_{\text{egr}}, 0)$$
$$- X_{\text{Oem}} \max(-W_{\text{t}}, 0)\big)$$

Intake Throttle

$$W_{\text{th}} = \frac{p_{\text{ic}} \, \Psi_{\text{th}}(\Pi_{\text{th}}) A_{\text{th,max}} f_{\text{th}}(u_{\text{th}})}{\sqrt{T_{\text{im}} \, R_{\text{a}}}}$$

$$\Psi_{\text{th}}(\Pi_{\text{th}}) = \begin{cases} \Psi_{\text{th}}^*(\Pi_{\text{th}}) & \text{if } \Pi_{\text{th}} \leq \Pi_{\text{th,lin}} \\[2mm] \Psi_{\text{th}}^*(\Pi_{\text{th,lin}}) \frac{1 - \Pi_{\text{th}}}{1 - \Pi_{\text{th,lin}}} & \text{if } \Pi_{\text{th,lin}} < \Pi_{\text{th}} \end{cases}$$

$$\Psi_{\text{th}}^*(\Pi_{\text{th}}) = \sqrt{\frac{2 \, \gamma_{\text{th}}}{\gamma_{\text{th}} - 1} \left(\Pi_{\text{th}}^{2/\gamma_{\text{th}}} - \Pi_{\text{th}}^{1 + 1/\gamma_{\text{th}}} \right)}$$

$$\Pi_{th} = \begin{cases} \left(\frac{2}{\gamma_{\text{th}} + 1} \right)^{\frac{\gamma_{\text{th}}}{\gamma_{\text{th}} - 1}} & \text{if } \frac{p_{\text{im}}}{p_{\text{ic}}} < \left(\frac{2}{\gamma_{\text{th}} + 1} \right)^{\frac{\gamma_{\text{th}}}{\gamma_{\text{th}} - 1}} \\[3mm] \frac{p_{\text{im}}}{p_{\text{ic}}} & \text{if } \left(\frac{2}{\gamma_{\text{th}} + 1} \right)^{\frac{\gamma_{\text{th}}}{\gamma_{\text{th}} - 1}} \leq \frac{p_{\text{im}}}{p_{\text{ic}}} \leq 1 \\[3mm] 1 & \text{if } 1 < \frac{p_{\text{im}}}{p_{\text{ic}}} \end{cases}$$

$$f_{\text{th}}(u_{\text{th}}) = b_{\text{th1}}(1 - \cos(\min(a_{\text{th1}} \, u_{\text{th}} + a_{\text{th2}}, \pi))) + b_{\text{th2}}$$

Cylinder

Cylinder Flow

$$W_{\text{ei}} = \frac{\eta_{\text{vol}} \, p_{\text{im}} \, n_{\text{e}} \, V_{\text{d}}}{120 \, R_{\text{a}} \, T_{\text{im}}}$$

$$\eta_{\text{vol}} = c_{\text{vol1}} \frac{r_{\text{c}} - \left(\frac{p_{\text{em}}}{p_{\text{im}}} \right)^{1/\gamma_{\text{e}}}}{r_{\text{c}} - 1} + c_{\text{vol2}} \, W_{\text{f}}^2 + c_{\text{vol3}} \, W_{\text{f}} + c_{\text{vol4}}$$

$$W_{\text{f}} = \frac{10^{-6}}{120} \, u_{\delta} \, n_{\text{e}} \, n_{\text{cyl}}$$

$$W_{\text{eo}} = W_{\text{f}} + W_{\text{ei}}$$

$$\lambda = \frac{W_{\text{ei}} \, X_{\text{Oim}}}{W_{\text{f}} \, (\text{O/F})_{\text{s}} X_{\text{Oc}}},$$

where X_{Oc} is the constant oxygen concentration in air, i.e. 23%.

$$X_{\text{Oe}} = \frac{W_{\text{ei}} \, X_{\text{Oim}} - W_{\text{f}} \, (\text{O/F})_{\text{s}}}{W_{\text{eo}}}$$

Exhaust Manifold Temperature

Cylinder out temperature

$$T_e = T_{im} + \frac{q_{HV}\, f_{Te}(W_f, n_e)}{c_{pe}\, W_{eo}}$$

$$f_{Te}(W_f, n_e) = f_{TeWf}(W_f) \cdot f_{Tene}(n_e)$$
$$f_{TeWf}(W_f) = c_{fTeWf1}\, W_{f,norm}^3 + c_{fTeWf2}\, W_{f,norm}^2 + c_{fTeWf3}\, W_{f,norm} + c_{fTeWf4}$$
$$f_{Tene}(n_e) = c_{fTene1}\, n_{e,norm}^2 + c_{fTene2}\, n_{e,norm} + 1$$

$$W_{f,norm} = W_f \cdot 100, \quad n_{e,norm} = \frac{n_e}{1000}$$

Heat losses in the exhaust pipe

$$T_{em,in} = T_{amb} + (T_e - T_{amb})\, e^{-\frac{h_{tot}\, \pi\, d_{pipe}\, l_{pipe}\, n_{pipe}}{W_{eo}\, c_{pe}}}$$

EGR-Valve

$$W_{egr} = \begin{cases} \dfrac{A_{egr}\, p_{em}\, \Psi_{egr}\left(\frac{p_{im}}{p_{em}}\right)}{\sqrt{T_{em}\, R_e}} & \text{if } p_{em} \geq p_{im} \\[3ex] -\dfrac{A_{egr}\, p_{im}\, \Psi_{egr}\left(\frac{p_{em}}{p_{im}}\right)}{\sqrt{T_{egr,cool}\, R_a}} & \text{if } p_{em} < p_{im} \end{cases}$$

$$\Psi_{egr}(\Pi_{egr}) = 1 - \left(\frac{1 - \Pi_{egrlim}(\Pi_{egr})}{1 - \Pi_{egropt}} - 1\right)^2$$

$$\Pi_{egrlim}(\Pi_{egr}) = \begin{cases} \Pi_{egropt} & \text{if } \Pi_{egr} < \Pi_{egropt} \\[2ex] \Pi_{egr} & \text{if } \Pi_{egr} \geq \Pi_{egropt} \end{cases}$$

$$A_{egr} = A_{egrmax}\, f_{egr}(u_{egr})$$

$$f_{egr}(u_{egr}) = b_{egr1}(1 - \cos(\min(a_{egr1}\, u_{egr} + a_{egr2}, \pi))) - b_{egr1}(1 - \cos(\min(a_{egr2}, \pi)))$$

Turbocharger

Turbo Inertia

$$\frac{d}{dt}\omega_t = \frac{P_t\, \eta_m - P_c}{J_t\, \omega_t}$$

Turbine Efficiency

$$P_t \, \eta_m = \eta_{tm} \, P_{t,s} = \eta_{tm} \, W_t \, c_{pe} \, T_{em} \left(1 - \Pi_t^{1-1/\gamma_e} \right)$$

$$\eta_{tm} = \eta_{tm,BSR}(BSR) \cdot \eta_{tm,\omega_t}(\omega_t) \cdot \eta_{tm,u_{vgt}}(u_{vgt})$$

$$\eta_{tm,BSR}(BSR) = 1 - b_{BSR} \left(BSR^2 - BSR_{opt}^2 \right)^2$$

$$BSR = \frac{R_t \, \omega_t}{\sqrt{2 \, c_{pe} \, T_{em} \left(1 - \Pi_t^{1-1/\gamma_e} \right)}}$$

$$\eta_{tm,\omega_t}(\omega_t) = \begin{cases} 1 - b_{\omega t1} \, \omega_t & \text{if } \omega_t \leq \omega_{t,lim} \\ 1 - b_{\omega t1} \, \omega_{t,lim} - b_{\omega t2}(\omega_t - \omega_{t,lim}) & \text{if } \omega_t > \omega_{t,lim} \end{cases}$$

$$\eta_{tm,u_{vgt}}(u_{vgt}) = b_{vgt1} \, u_{vgt}^3 + b_{vgt2} \, u_{vgt}^2 + b_{vgt3} \, u_{vgt} + b_{vgt4}$$

$$\Pi_t = \frac{p_t}{p_{em}}$$

Turbine Mass-Flow

$$W_t = \frac{A_{vgtmax} \, p_{em} \, f_{\Pi t}(\Pi_t) f_{\omega t}(\omega_{t,corr}) \, f_{vgt}(u_{vgt})}{\sqrt{T_{em} \, R_e}}$$

$$f_{\Pi t}(\Pi_t) = \sqrt{1 - \Pi_t^{K_t}}$$

$$f_{\omega t}(\omega_{t,corr}) = 1 - c_{\omega t} \left(\omega_{t,corr} - \omega_{t,corropt} \right)^2$$

$$\omega_{t,corr} = \frac{\omega_t}{100\sqrt{T_{em}}}$$

$$f_{vgt}(u_{vgt}) = c_{f2} + c_{f1} \sqrt{\max \left(0, 1 - \left(\frac{u_{vgt} - c_{vgt2}}{c_{vgt1}} \right)^2 \right)}$$

Compressor Efficiency

$$P_c = \frac{P_{c,s}}{\eta_c} = \frac{W_c \, c_{pa} \, T_{amb}}{\eta_c} \left(\Pi_c^{1-1/\gamma_a} - 1 \right)$$

$$\Pi_c = \frac{p_{ic}}{p_{amb}}$$

$$\eta_c(W_{c,corr}, \Pi_c) = \eta_{c,W}(W_{c,corr}, \Pi_c) \cdot \eta_{c,\Pi}(\Pi_c)$$

$$\eta_{c,W}(W_{c,corr}, \Pi_c) = 1 - a_{W3}(W_{c,corr} - (a_{W1} + a_{W2} \, \Pi_c))^2$$

$$\eta_{c,\Pi}(\Pi_c) = \begin{cases} a_{\Pi 1} \, \Pi_c^2 + a_{\Pi 2} \, \Pi_c + a_{\Pi 3} & \text{if } \Pi_c < \Pi_{c,lim} \\ a_{\Pi 4} \, \Pi_c^2 + a_{\Pi 5} \, \Pi_c + a_{\Pi 6} & \text{if } \Pi_c \geq \Pi_{c,lim} \end{cases}$$

$$a_{\Pi 6} = \Pi_{c,lim}^2(a_{\Pi 1} - a_{\Pi 4}) + \Pi_{c,lim}(a_{\Pi 2} - a_{\Pi 5}) + a_{\Pi 3}$$

$$W_{c,corr} = \frac{W_c \, \sqrt{(T_{amb}/T_{ref})}}{(p_{amb}/p_{ref})}$$

Compressor Mass-Flow

$$W_c = \frac{p_{amb} \, \pi \, R_c^3 \, \omega_t}{R_a \, T_{amb}} \Phi_c$$

$$\Psi_c = \frac{2 \, c_{pa} \, T_{amb} \left(\Pi_c^{1-1/\gamma_a} - 1 \right)}{R_c^2 \, \omega_t^2}$$

$$\Phi_c = \frac{k_{c1} - k_{c3} \, \Psi_c}{k_{c2} - \Psi_c}$$

$$k_{ci} = k_{ci1} \left(\min(Ma, Ma_{max}) \right)^2 + k_{ci2} \, \min(Ma, Ma_{max}) + k_{ci3}, \quad i = 1, \ldots, 3$$

$$Ma = \frac{R_c \, \omega_t}{\sqrt{\gamma_a \, R_a \, T_{amb}}}$$

Table B.1. Symbols used in the plant model.

Symbol	Description	Unit
A	Area	m^2
BSR	Blade speed ratio	–
c_p	Spec. heat capacity, constant pressure	J/(kg·K)
c_v	Spec. heat capacity, constant volume	J/(kg·K)
J	Inertia	kg· m^2
n_{cyl}	Number of cylinders	–
n_e	Rotational engine speed	rpm
p	Pressure	Pa
P	Power	W
q_{HV}	Heating value of fuel	J/kg
r_c	Compression ratio	–
R	Gas constant	J/(kg·K)
R	Radius	m
T	Temperature	K
u_{egr}	EGR control signal[†]	%
u_{th}	Throttle control signal[†]	%
u_{vgt}	VGT control signal[†]	%
u_δ	Injected amount of fuel	mg/cycle
V	Volume	m^3
W	Mass flow	kg/s
γ	Specific heat capacity ratio	–
η	Efficiency	–
Π	Pressure quotient	–
ρ	Density	kg/m^3
Φ_c	Volumetric flow coefficient	–
Ψ_c	Energy transfer coefficient	–
ω	Rotational speed	rad/s

[†] 0 – closed, 100 – open

Table B.2. Indices used in the plant model.

Index	Description
a	air
amb	ambient
c	compressor
d	displaced
e	exhaust
egr	EGR
ei	engine cylinder in
em	exhaust manifold
eo	engine cylinder out
ic	intercooler
f	fuel
im	intake manifold
t	turbine
th	throttle
vgt	VGT
vol	volumetric
δ	fuel injection

Table B.3. States, inputs, and outputs of the plant model.

States	Inputs	Outputs
p_{im}	u_{δ}	p_{im}
p_{em}	u_{th}	p_{em}
p_{ic}	u_{egr}	p_{ic}
ω_{t}	u_{vgt}	ω_{t}
T_{em}	n_{e}	W_{c}